The structure and long-term variation of the stratospheric circulation

学位論文（要約）

The structure and long-term variation of the stratospheric circulation

（　成層圏大循環の構造と長期変動　）

平成 25 年 7 月 博士 (理学) 申請

東京大学大学院理学系研究科

地球惑星科学専攻

岡本功太

Contents

Abstract 10

Abstract (in Japanese) 14

1 General Introduction 18

1.1 The mean meridional circulation in the middle atmosphere 18

1.1.1 Gravity waves 19

1.1.2 Gravity waves in models 20

1.1.3 The residual mean circulation 22

1.1.4 The role of wave-induced force in the residual mean circulation 23

1.2 Roles of gravity waves in the mean meridional circulation change . 24

1.2.1 BDC trends in the GHG increase 24

1.2.2 Response to the ozone depletion 26

1.2.3 Remote interaction in the middle atmosphere 28

1.3 Purpose of this study 30

2 Roles of atmospheric waves on the Brewer-Dobson circulation 33

2.1 Data description 34
2.2 Indirect estimation method of GW contribution 35
2.2.1 GW contribution to the residual mean circulation 36
2.2.2 GW contribution to the tropical upward mass flux 38
2.3 Results 38
2.3.1 GW contribution to the formation of the BDC 39
2.3.2 GW contribution to the strength of the BDC 41
2.3.3 GW contribution to the structure of the BDC 43
2.3.4 GW contribution to the seasonal variation of the BDC 44
2.4 Summary 48

3 Effects of the ozone and CO_2 trends on the early summer SH middle atmosphere 50
3.1 WACCM data description 51
3.2 MLT trends in the early summer during the ozone increase period 54
3.2.1 Response observed below the mesopause 54
3.2.2 Response observed above the mesopause 59
3.3 The ozone and CO_2 trend contributions to the MLT trends 62
3.3.1 Comparison between different RCPs 62
3.3.2 A multiple linear regression analysis 64
3.4 Summary 66

4 A dynamical coupling between the SAO and PNJ in austral winter 69
4.1 Data description 71

4.1.1 High-resolution GCM data 71
4.1.2 Reanalysis data 72
4.2 Seasonal variation in the austral winter 73
4.2.1 TEM analysis 73
4.2.2 Mean winds and temperature 74
4.2.3 Seasonal variation observed in the high-resolution GCM data . 75
4.2.4 Seasonal variation observed in the reanalysis data 80
4.3 Interannual variability of SAO and PNJ in reanalysis data 83
4.3.1 Composite analysis 85
4.3.2 Composite on the SAO variability 86
4.3.3 Composite on the PNJ variability 92
4.3.4 Discussion: A possible interaction between SAO and PNJ variability 94
4.4 Summary 98

5 General conclusions 100

Acknowledgments 116

List of Figures

1.1 (a) A schematic illustration of the mean meridional circulation (arrows) in the latitude-height cross section described by Plumb (2002). Regions where atmospheric waves are breaking are shaded. “S”, “P”, and “G” denote the synoptic-scale waves, the planetary waves, and the gravity waves, respectively. (b) Monthly mean meridional distribution of $\mathrm{CH_4}$ [ppm] during March from satellite observations adopted from Randel et al. (1998). 19

1.2 (a) A meridional cross section of momentum flux associated with gravity waves [mPa] (colors) and zonal mean zonal wind [$\mathrm{ms^{-1}}$] (contour) in July simulated by a gravity wave-resolving GCM. (b) Rays of gravity waves (thin curves) in the idealized background westerly winds [$\mathrm{ms^{-1}}$] (contours). Adopted from Sato et al. (2009). 22

1.3 Linear trends in (a) temperature (units: $\mathrm{K/47years}$; contour intervals 4), (b) zonal wind (units: $\mathrm{m/s/47years}$; contour intervals 4), (c) gravity wave drag (units: $\mathrm{m/s/day/47years}$; contour intervals 8), (d) residual mean meridional flow (units: $\mathrm{m/s/47years}$; contour intervals 0.4), and (e) residual mean vertical flow (units: $\mathrm{cm/s/47years}$; contour intervals 0.2) over the period 1960-2006 averaged over the months of November and December. Negative contours are dashed and zero contours are not drawn. Adopted from Smith et al. (2010). 27

2.1 Meridional cross sections of (a) zonal mean zonal wind (contour) and zonal mean temperature, and (b) the stream function of the residual mean circulation averaged for July in 1990-2002 calculated from ERA-Interim data. Contour interval is 10 $\mathrm{ms^{-1}}$ for (a). 36

2.2 Meridional cross sections of (left panels) the stream function of the residual circulation, and contributions of (center panels) resolved wave forcing and (right panels) gravity wave forcing as a residual, for (upper panels) January and (lower panels) July calculated from the ERA-Interim data. 40

2.3 (a) Annual mean tropical upward mass flux at 70 hPa (green) and contributions of the resolved wave forcing (blue) and gravity wave forcing (red) for the ERA-Interim data. NH and SH components are plotted in (b) and (c), respectively. 42

2.4 The stream function of the residual circulation at 70 hPa (black curves) and contributions of the resolved wave forcing (blue) and gravity wave forcing (red) are plotted as a function of latitude for the the ERA-Interim data. 43

2.5 Time-height cross section of the total tropical upward mass flux for the ERA-Interim data. Contours are for 20, 30, 50, and 100 kgs^{-1}. . . 45

2.6 Time series of monthly-mean total upward mass flux (black curves), NH component (red curves), and SH component averaged for the period of 1990-2002 at (a) 70 hPa and (b) 10 hPa. 46

2.7 The stream function of the residual circulation at 10 hPa (black curves) and contributions of the resolved wave forcing (blue) and gravity wave forcing (red) are plotted as functions of latitude for ERA-Interim data. 47

3.1 Time series of (a) ozone mixing ratio averaged in 80°S-90°S and (b) globally averaged CO_2 mixing ratio, at 72 hPa in November and December for RCP 8.5 (red curves), RCP 4.5 (black curves), and RCP 2.6 (blue curves). Meridional cross sections of the average and trend in (c) the ozone mixing ratio and (d) CO_2 mixing ratio for RCP 4.5. The averages and trends are calculated for the period of 2015-2024 and 2015-2090, respectively, after averaged in November and December. 53

3.2 (Upper panels) The ozone trend in 80°-90°S, 72 hPa in the year-year sections for (left) RCP 2.6, (center) RCP 4.5, and (right) RCP 8.5. The horizontal and vertical axes show the beginning and the end, respectively, of a period for which the trend is calculated. (Middle panels) Same as in upper panels but for globally averaged CO_2 trend at 72 hPa. (Bottom panels) Same as in middle panels, but for the percentage change in the CO_2. 55
3.3 Time series of zonal mean temperature (thick-solid curve) and ozone mixing ratio (thin-solid curve) at 72 hPa averaged in 80°S-90°S in December for RCP 4.5 with linearly regressed lines. 56
3.4 Meridional cross sections of trend (colors) and average (contours) for (a) zonal mean temperature, (b) zonal mean zonal wind, (c) parameterized GW drag, (d) the residual meridional velocity, and (e) the residual vertical velocity. Linear trend is calculated for 76 early summers (November-December) in 2015-2090, and average is calculated for 10 early summers (November-December) in 2015-2024. . 57
3.5 Vertical distributions of (a) momentum flux associated with parameterized GW averaged for the period of 2015-2030 (solid curves) and 2075-2090 (dashed curves), and (b) its trend for westward component (blue curve), and eastward component (red curve) for the period of 2015-2090. The trends are calculated as a linear trend of 2015-2090 divided by average for 2015-2024, showing a percentage change relative to the past average. Zonal wind distributions for the same periods are also plotted by black curves in the left panel. Fluxes and zonal wind are averaged in 60°S-75°S for November and December. 59
3.6 Vertical distributions of (a) zonal mean temperature and (b)its change, averaged for NH summer polar region (blue curves), and SH summer polar region (red curves). Solid (dashed) curves are plotted as an average for the period of 2015-2030 (2075-2090) in the left panel. Values are averaged in 70°-90° in each hemisphere. . . . 60
3.7 Time series of zonal mean temperature (solid curves) and vertical component of the residual velocity (dashed curves) at 0.018 hPa (thick curves), and 0.0003 hPa (thin curves) averaged in 80°S-90°S in December for RCP 4.5. Regressed lines with significant trend are superimposed. 61

3.8 Meridional cross sections of trend (colors) and average (contours) for (left panels) CO_2 mixing ratio, (center panels) zonal mean temperature, (right panels) the vertical component of the residual mean circulation. The results for RCP 2.6 (RCP 8.5) are placed in the upper (lower) panels. Linear trend is calculated for 76 early summers (November-December) in 2015-2090, and average is calculated for 10 early summers (November-December) in 2015-2024. 63

3.9 Time series of zonal mean temperature (black-solid curve), the ozone mixing ratio (red curve), CO_2 mixing ratio (blue curve), and the temperature induced from the ozone and CO_2 variations (dashed curve) at 72 hPa averaged in 70°S-90°S in November and December for RCP 4.5 65

3.10 Meridional cross sections of the proportion of the regression coefficient for ozone to the regression coefficient for CO_2, for (a) RCP 2.6, (b) RCP 4.5, and (c) RCP 8.5. The rates are plotted for the region where the correlation coefficient between T and $\hat{T}$ is larger than 0.5 (correlation 0.8 is shown by contours). See text for details. 66

4.1 Meridional cross sections of the zonal mean zonal wind (contour) and the zonal mean temperature (color) averaged for June, July, and August for (a) simulation by GCM and (b) MERRA. The contour interval is 20 ms^{-1}. 75

4.2 Meridional cross sections of the monthly mean zonal mean zonal wind for (a) May, (b) June, (c) July, and (d) August in the GCM. The contour interval is 20 ms^{-1}. Easterlies are shaded. 76

4.3 Meridional cross sections of E-P flux divergence for (a)-(d) all resolved waves, (e)-(h) planetary-scale waves and (i)-(l) gravity waves for May, June, July, and August in the GCM. E-P flux vectors for planetary waves are superimposed on the middle panels. Monthly mean zonal mean zonal wind [ms^{-1}] is shown by contours and zero wind contours are plotted using red curve. 77

4.4 Same as in Figure 4.3 except for (a)-(d) the meridional component [$\times 10^{-1}\mathrm{ms}^{-1}$] and (e)-(h) the vertical component [$2 \times 10^{-4}\mathrm{ms}^{-1}$] of the residual mean circulation in the GCM. Contours in top panels show the absolute angular momentum [$\times 10^{8}\mathrm{m}^{2}\mathrm{s}^{-1}$], and those in bottom panels show the zonal wind same as in Figure 4.3. 78

4.5 Same as in Figure 4.2 but for the MERRA data for (a)-(d) 1982, (e)-(h) 1991, (i)-(l) 1996, and (m)-(p) 2009. 81
4.6 Meridional cross sections of (a)-(d) $\hat{f}\overline{v}^*$ [$\mathrm{ms}^{-1}\mathrm{day}^{-1}$], (e)-(h) planetary wave component of the E-P flux divergence [$\mathrm{ms}^{-1}\mathrm{day}^{-1}$], and the vertical component of the residual mean circulation [$2 \times 10^{-4}\mathrm{ms}^{-1}$] for May, June, July, and August in 1996. Monthly mean zonal mean zonal wind [ms^{-1}] is shown by contours. E-P flux vectors for planetary waves are superimposed on the middle panels . 82
4.7 Scatter diagrams for (a) equatorial zonal wind speed and SAOE height and (b) PNJ core latitude and height. Monthly mean values for July are plotted. The equatorial zonal wind speed is averaged in a region of 15°S-5°N and 43-57 km. 84
4.8 Scatter diagrams for (a) SAOE height and PNJ core height; (b) SAOE height and PNJ core latitude; (c) equatorial zonal wind speed and PNJ core height; and (d) equatorial zonal wind speed and PNJ core latitude. 85
4.9 Time series of (a) minimum of the zonal mean zonal wind averaged in 15°S-5°N and 43-57 km; and (b) PNJ core height for July. 86
4.10 Meridional cross sections of (a)-(c) temperature, (d)-(f) $-\hat{f}\overline{v}^*$, (g)-(i) the planetary wave forcing, and (j)-(l) $\overline{w}^*$ averaged for (left panels) S-SAOE Julys, (center panels) W-SAOE Julys, and (right panels) their differences. The E-P flux vectors associated with the planetary wave component are superimposed on the planetary wave forcing. Contours show absolute angular momentum for (d)-(f) and zonal mean zonal wind for others. 88
4.11 Latitude-relative height from the SAOE height cross sections of (a) temperature, (b) $-\hat{f}\overline{v}^*$, (c) the planetary wave forcing, (d) $\overline{w}^*$ averaged for S-SAOE Julys. 91
4.12 Same as in Figure 4.10 but for (left panels) L-PNJ Julys, (middle panels) H-PNJ Julys, and (right panels) their differences. 93
4.13 Schematic illustrations of the middle atmosphere residual circulation and zonal wind distribution for (a) climatology, (b) anomaly in the S-SAOE case, and (c) anomaly in the L-PNJ case. 95

Abstract

The meridional circulation in the stratosphere called the Brewer-Dobson circulation (BDC) consisting of tropical upwelling and extratropical downwelling was found from the observations of ozone and water vapor distributions. Recent studies indicated that the BDC is composed of deep and shallow branches. The former extends up to the upper stratosphere and the latter is confined in the lower stratosphere. This circulation is approximately expressed by the residual circulation in the transformed Eulerian mean (TEM) system, although isentropic mixing is also important for the distribution of minor constituents. In the TEM framework, the BDC is driven by a body force associated with breaking/dissipation of the atmospheric waves. The deep branch is driven by the planetary wave forcing, while the shallow branch is driven by the synoptic-scale waves. Recent studies suggested the important role of the gravity wave on the BDC. However, because of their small scales, the estimation of the global distribution of the gravity wave forcing from observations is generally difficult and hence gravity wave parameterizations used in most climate models are based on uncertain assumptions. In this study, we first examine the contribution of gravity waves to BDC by a diagnostic method using reanalysis data sets which include gravity wave effects in large-scale fields through assimilation of huge amount of observational data.

The gravity wave (GW) contribution to the BDC is indirectly estimated using the downward control principle under an assumption of the steady state. This method is applied to four analyses to examine the stratospheric residual mean circulation for the ERA-Interim reanalysis data. First, the GW contribution to the formation of the residual circulation is examined. The results show that the deep branch in the summer subtropics is mainly driven by GWs.

Second, the GW contribution to the tropical upward mass flux in the lower stratosphere is investigated. GWs contribute to about 30% of the total mass flux, which is consistent with previous studies. Next, the GW effects are investigated on the determination of the turnaround latitude (TL) in the lower stratosphere, which is defined as a latitude of zero vertical velocity. The stream function contributed by the resolved wave forcing is not maximized near the TL, suggesting the importance of the GW for determining the location of TL. Finally, seasonal variations of the tropical upward mass flux are examined. The mass flux in the lower stratosphere exhibits annual cycle, while semiannual cycle is dominant in the middle stratosphere. It is considered that this difference between the two height regions is caused by three points. One is the GW contribution which increases with height. The other two are the interhemispheric differences in the planetary wave activity and in the persistency of westerly wind in the lower stratosphere. These results indicate the importance of the gravity waves for the formation and seasonal variation of the BDC even in the lower and middle stratosphere.

Long-term change of the meridional circulation in the middle atmosphere is another interesting topic. Recent studies focusing on the future climate change associated with increasing greenhouse gases and a decreasing trend of ozone depleting substances reported an acceleration of the BDC in the mid-21st century. In addition, dynamical response of the mesosphere-lower thermosphere (MLT) region to the ozone depletion trend in the polar stratosphere in the late 20th century was also examined. In this thesis, the remote dynamical responses to ozone recovery and CO_2 increase in the 21st century are examined using data from chemistry-climate model simulations.

In early summer, ozone recovery in the lower stratosphere results in a temperature increase in the polar lower stratosphere, leading to an easterly trend in the whole stratosphere. The change in the wind distribution allows propagation of more gravity waves into the mesosphere so that the mesospheric residual mean circulation is intensified by the gravity wave drag. The consequent polar temperature trend below the mesopause is negative due to the adiabatic re-

sponse to the positive trend in the upwelling. This response is opposite to that of the ozone loss in the 20th century and hence the present study supports the mechanism proposed by previous studies. However, the temperature response in the lower thermosphere is not consistent with the expected adiabatic change. To examine the mechanism of the temperature response, other simulation data with three scenarios for the CO_2 variation in the 21st century are used. From comparisons of the positive CO_2 trend cases and no CO_2 trend case, the mesospheric temperature trend is mainly attributed to the ozone increase in the lower stratosphere, while the CO_2 trend largely affects the temperature response in the lower thermosphere. In addition, this result is supported by the multiple linear regression analysis.

In the equatorial atmosphere, unique oscillations called the quasi-biennial oscillation (QBO) and semiannual oscillation (SAO) are observed in the zonal mean zonal wind. It is known that the QBO affects the strength of the polar night jet (PNJ) and the frequency of the sudden stratospheric warming. However, dynamical connection between the SAO and PNJ has not been examined in detail so far. Thus, this study made an analysis from this view point using high resolution general circulation model (GCM) data and a reanalysis dataset. In particular, analysis was focused on the austral winter.

First, the GCM and reanalysis data are examined to investigate the seasonal march during austral winter. The PNJ core and easterly phase associated with the SAO descend with time. It seems that two descents are synchronized. Such a feature is also observed in several years in the reanalysis data. In addition, strong upwelling is located in the upper stratosphere and lower mesosphere, which is above and lower latitude side of PNJ core. This upwelling may affect the zonal wind distribution through the temperature change by adiabatic cooling. Next, long-term reanalysis data is used to examine the PNJ-SAO relation in the interannual variability focusing on July. All Julys are divided into two groups (strong SAO easterly Julys and weak SAO easterly Julys) and averaged for each group. From the comparison of two groups, more planetary waves tend to break around the SAO easterly and drive the strong poleward

flow in the upper stratosphere in the mid-latitudes for the strong SAO easterly Julys than for the weak SAO easterly Julys. In addition, equatorial flow anomaly in the subtropical mesosphere is observed in the strong SAO easterly Julys. These two flow anomalies are combined into the strong upwelling in the mid-latitude upper stratosphere and lower mesosphere. This strong upwelling can affect the upper part of the PNJ through the temperature change. It is also found that the PNJ core height is located around the height of SAO easterly from the composite analysis based on the height of SAO easterly. On the other hand, composite analysis on the PNJ core height suggests that more planetary waves tend to propagate into the SAO easterly region in the lower PNJ core height Julys, which can enhance the easterly wind in the subtropics. These results indicate that the SAO variability affects the PNJ variability through the residual circulation change in the mid-latitudes, and the PNJ variability also affects the SAO variability through the control of the planetary wave propagation, which may adjust the location of the SAO easterly phase and the PNJ core.

The present study examined the variation and interaction of the residual mean circulation and various kinds of waves mainly in the meridional cross section in the two dimensional TEM framework. However, several recent studies indicate that the stratospheric circulation has longitudinally-dependent three-dimensional structure. It is also known from recent satellite observations that the stratopause and PNJ are not zonally uniform. Moreover, a three-dimensional TEM equation system has recently been developed, which treats both gravity waves and Rossby waves. For the future work, as an extension of the present study the three-dimensional aspects of the structure, seasonal variation, and long-term variation of the residual mean circulation in the middle atmosphere should be investigated.

要旨

成層圏には赤道から極へと向かうゆっくりとした子午面循環 (Brewer-Dobson 循環: BDC) が存在することがオゾンや水蒸気の観測から明らかになっている。さらに近年の研究では BDC が上部成層圏まで達するような深い循環と下部成層圏に制限される浅い循環によって構成されることが知られている。この子午面循環は変形オイラー平均 (Transformed Eulerian mean: TEM) 系の残差子午面循環で近似的に表現することができる。TEM 系を用いた解析により、成層圏を含む中層大気の循環は大気波動の砕波や散逸による強制によって駆動されていることがわかっている。深い循環は主に下層から成層圏中緯度域に伝播してくるプラネタリー波の砕波や散逸に伴う強制によって、また浅い循環は主に上部対流圏及び下部成層圏の総観規模波動によって駆動されることが知られている。大気重力波も重要な役割を果たすことが様々な研究から明らかになってきているが、一方で観測の難しさや大気大循環モデルにおけるパラメタリゼーションの不完全性などから定量的評価は一般に難しい。そこで本研究ではまず、重力波の寄与を含んだ場を再現する再解析データから診断的に重力波の寄与を推定することで成層圏循環における重力波の役割を示す。

残差循環は東西平均流とストークスドリフトの和で表現される。解像される波の寄与は再解析データで直接計算できる。一方ダウンワードコントロールの原理を用いると、定常状態では残差循環を波強制のみを用いて計算することができる。さらに、波強制は様々なスケールの波の線形和で表すことができる。したがって、重力波の寄与は直接計算される残差循環とダウンワードコントロールを用いて推定される解像される波の寄与との差として推定することが可能となる。この手法を ERA-Interim 再解析データの 1990-2002 年に適用して成層圏残差循環に対する 4 つの解析を行った。最初に、子午面断面における流線

関数への波強制の寄与を比較することで BDC の形成に関する波の役割を確認した。ここでは先行研究どおり、冬半球の深い循環は主にプラネタリー波が、両半球の浅い循環は総観規模波動が駆動することが確認された。さらに、夏半球低緯度の深い循環の上昇流と下部成層圏中緯度の浅い循環は主に重力波が駆動していることがわかった。この結果は他の再解析データとも比較してみたが整合的であった。次に BDC の強さの指標の一つである熱帯上向き質量フラックスを計算し、それぞれの波強制の寄与を調べたところ、重力波の寄与が 30% 程度あることがわかった。さらに、質量フラックスの決定に重要なパラメータであるターンアラウンド緯度 (TL: 流線関数が極大もしくは極小となる緯度) についても解析を行った。70 hPa の流線関数の大きさはほぼ解像波によって決まっているが、解像波の駆動する循環の流線関数は TL 付近では勾配が小さく極大極小を作ることができない。したがってこの結果は、TL を決める流線関数の極大極小は残差として推定された重力波の寄与の影響が大きいことを示唆している。最後に、質量フラックスの季節変化について調べた。質量フラックスは下部成層圏では 1 年周期の変動をするのに対し、中部成層圏では半年周期の変動をすることがわかった。北半球と南半球の成分はともに 1 年周期で冬に最大となるような季節変化をする。下部成層圏では北半球成分の振幅が南半球成分よりも大きいために全質量フラックスの変動は北半球成分の変動と正相関となる。一方、中部成層圏では、北半球と南半球の振幅が同程度で、全質量フラックスの変動は半年周期に近くなる。これら高さによる違いはプラネタリー波活動度の半球間の違いや下部成層圏で西風が続く期間の長さ、重力波の寄与の高さによる違いで説明できる可能性がある。以上 4 つの解析は、下部から中部成層圏においても重力波が成層圏循環に対して重要な役割を持つことを示唆している。

近年、成層圏気候の将来予測が盛んに行われ、温室効果ガス増加に対して成層圏循環が加速することや、オゾンホールが今世紀中頃には消滅することなどが様々な気候モデルから報告されている。また、20 世紀の南半球極域ではオゾンホール発達期にオゾントレンドと中間圏下部熱圏温度トレンドとの関連も示唆されている。本研究では将来予測されるオゾンと温室効果ガスのトレンドと成層圏循環の変化に対する上部成層圏から下部熱圏の

応答と大気波動の役割についてアメリカ大気研究所 (NCAR) の気候モデル WACCM を用いて調べた。

21 世紀のオゾン回復と二酸化炭素トレンドに対する中間圏下部熱圏の力学的応答について解析を行った。初夏の南極域下部成層圏はオゾン増加トレンドを受けて高温偏差となり温度風の関係から成層圏は東風トレンドとなる。このとき、成層圏を通って中間圏へ達する重力波は正味で西風運動量をもつものが増える。すなわち、中間圏の赤道向き循環は加速トレンドとなる。この結果、中間圏極域では上昇流が強化され、低温トレンドが現れる。これは 20 世紀のオゾン減少トレンドに対する中間圏の応答を調べた先行研究と整合的である。一方下部熱圏の温度トレンドは下降流トレンドと整合的ではなく、これは非断熱的な応答が寄与している可能性を示唆している。そこで温室効果ガスの変化についての 3 つのシナリオを用いて計算されたデータを用いて、中間圏及び下部熱圏の長期的な応答に対する温室効果ガスとオゾントレンドの寄与を調べた。温室効果ガスが増加するシナリオと増加しないシナリオを比較した結果、中間圏の温度減少トレンドには下部成層圏のオゾン増加の影響が大きいことがわかった。また下部熱圏の応答はシナリオ間での差が顕著に現れた。これは温室効果ガストレンドの影響がこの領域で大きいことを示唆している。この結果は、極域下部成層圏オゾンの変動と二酸化炭素の変動を変数にとった温度変動についての多重回帰解析でも確認された。

熱帯中層大気の内部変動として下部成層圏準二年周期振動 (QBO) と上部成層圏半年周期振動 (SAO) がある。前者は先行研究により下部成層圏の極夜ジェットの強さに影響を与えうることが知られている。本研究では SAO が中高緯度大気に与えうる影響と大気波動の役割について、高解像度気候モデルと長期再解析データを用いて統計的に解析した。

まず、重力波解像気候モデルデータと再解析データを用いて、南半球の冬に着目して 5 月から 8 月にかけての時間変化の解析を行った。極夜ジェットは季節進行とともに高度を下げてき、また SAO に伴う東風も時間と共に下降する。気候モデルにおいては両者が高度をそろえて同期的に下降するように見え、また再解析データのいくつかの年においても同様の現象が見られた。残差循環や波強制の解析から、極夜ジェットのコアと SAO の

東風の間である上部成層圏中緯度域でプラネタリー波が駆動する極向きの強い流れと、極夜ジェット上部で重力波が駆動する極向きの強い流れ、また亜熱帯での弱い極向きまたは赤道向きの循環によって極夜ジェットコア上部赤道側に強い上昇流ができることがわかった。この上昇流は断熱的に温度に影響を与える可能性がある。またこの残差循環と波強制は SAO 東風と極夜ジェットとの相対的な位置を保ったまま季節進行している。次に、同じ再解析データを用いて 7 月に着目し、年々変動の解析を通して SAO 東風と極夜ジェットの関係を統計的に調べた。7 月の SAO 東風の強さと高度、極夜ジェットの位置の年々変動に相関が見られた。まず、SAO 東風に強さについて弱い年と強い年を抽出してそれぞれ平均し比較した。SAO 東風が強い年には中緯度上部成層圏でプラネタリー波が砕波しやすく、亜熱帯中間圏の循環には赤道向き偏差が見られた。さらに極夜ジェット上部低緯度側の上昇流が強化される傾向にあることがわかり、極夜ジェットのコアは SAO 東風が弱い年に比べてより極側下側に存在する。また、SAO 東風が強い年において SAO 東風の高度を基準として高度をずらして平均したところ極夜ジェットのコアと SAO 東風の位置がほぼ同じ高度にあることがわかった。次に極夜ジェットの高度についても高い年と低い年を定義しそれぞれでコンポジットをとって比較した。結果としては低い年の方がよりプラネタリー波が上部成層圏赤道向きに伝播する傾向にあり、低緯度域の東風は極夜ジェットが高い年に比べて強く、東風領域もより高緯度側へ広がる様子が見られた。これらの結果は極夜ジェットと SAO 東風の年々変動が大気波動を介してそれぞれの位置や強さに相互に影響を与えうる可能性を示唆している。

本研究の循環と大気波動の解析は、2 次元 TEM 系力学に基づいた緯度高度断面のみで行われた。しかし、最近の研究では成層圏循環が経度方向に依存性のある 3 次元的な構造を持つことを示している。また衛星観測などから、成層圏界面や極夜ジェットも東西に非一様であることがわかってきた。さらに近年、重力波とロスビー波の両者を扱える 3 次元 TEM 方程式系が開発されている。本研究の発展として中層大気残差循環の 3 次元的な構造や、季節変化、長期変動を詳しく解析したい。

Chapter 1

General Introduction

1.1 The mean meridional circulation in the middle atmosphere

The atmosphere including the stratosphere, mesosphere, and lower thermosphere from the height of 10 km to 120 km is called “the middle atmosphere”. In contrast to the troposphere, large meridional circulations are observed in the middle atmosphere. Figure 1.1a summarizes the mean global meridional circulation in the solstice season. In the stratosphere, the upwelling in the low latitudes, poleward flow in the mid-latitudes, and downwelling in the higher latitudes are dominant in both hemispheres throughout the year. The stratospheric meridional circulation is called the Brewer-Dobson circulation (BDC) after Brewer (1949) and Dobson (1952) for their observations of ozone and water vapor. In contrast to the stratosphere, in the mesosphere there is one-celled circulation from the summer pole to the winter pole followed by the upwelling in the summer high latitudes and the downwelling in the winter high latitudes. It is known that such circulations have some important roles in the middle atmosphere. In the middle atmosphere, the temperature structure is apart from that expected from the radiative equilibrium condition, which is maintained by the adiabatic heating/cooling due to the mean meridional circulation. In addition, mean meridional circulation can affect the material distribution by advection. Figure 1.1b shows the stratospheric and

(a) (b)

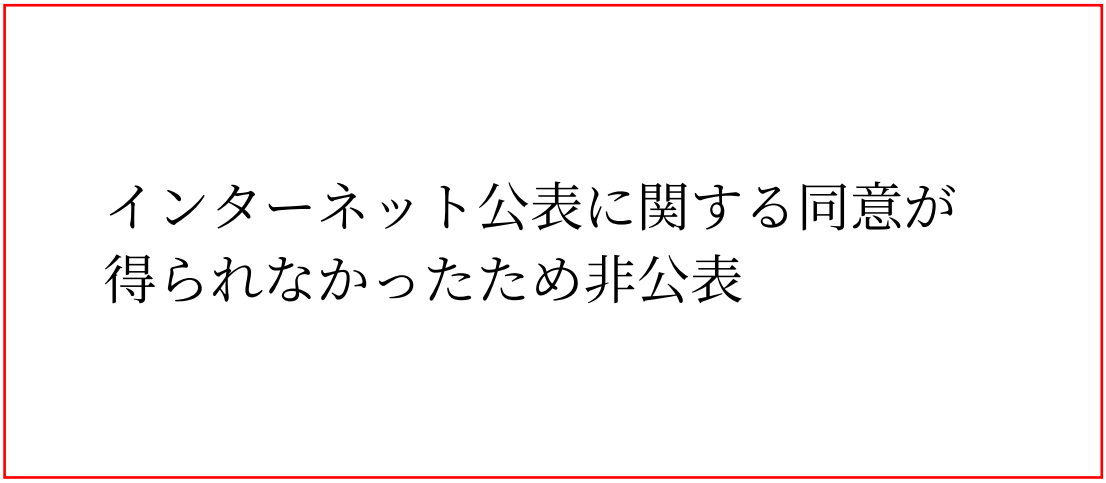

Fig. 1.1 (a) A schematic illustration of the mean meridional circulation (arrows) in the latitude-height cross section described by Plumb (2002). Regions where atmospheric waves are breaking are shaded. "S", "P", and "G" denote the synoptic-scale waves, the planetary waves, and the gravity waves, respectively. (b) Monthly mean meridional distribution of CH_4 [ppm] during March from satellite observations adopted from Randel et al. (1998).

lower mesospheric mean global distribution of the CH_4 obtained from the satellite observations. It is obvious that the material surfaces are raised in the low latitudes and pushed down in the higher latitudes, which is largely following the material transport by the mean meridional circulation. Thus, it is important to understand the dynamics of the mean meridional circulation in the middle atmosphere. One of the key factors to understand the mean meridional circulation is the atmospheric wave. It is considered that large part of the mean meridional circulation in the middle atmosphere is driven by the wave-induced force.

1.1.1 Gravity waves

One of the most important atmospheric waves for the middle atmosphere dynamics is the gravity wave. The gravity wave is sometimes called the buoyancy wave because the restoring force of the gravity wave is buoyancy. The gravity wave is considered to be generated from several kinds of sources such as airflow over high topography, front, jet stream, cyclone, and

convection (Fritts and Nastrom, 1992). The orographic gravity wave is excited when the stratified air flows over the irregular topography like a mountain causing a form drag, which is a well-known mechanism due to previous works (McFarlane, 1987; Holton and Hakim, 2013, e.g). An example of the source of convectively generated gravity waves is considered to be thermal forcing (Beres et al., 2002, 2004). The vertical width of the diabatic heating determines the scale of convectively generated gravity waves (Salby and Garcia, 1987). The gravity wave generated in fronts and jets have recently been investigated in many studies focusing on the spontaneous adjustment process (Zhang, 2004).

These gravity waves generated in the lower atmosphere freely propagate upward into the middle atmosphere conserving their energy before the breaking which occurs when/where they reach their critical levels or become unstable due to increased amplitude. The mechanism of the wave breaking has been studied by Lindzen (1981) from the linear saturation theory. The group velocity of the gravity wave becomes zero near the critical level where the phase speed of the gravity wave is equal to the background mean flow, causing wave breaking and momentum deposition to the mean flow (Holton and Hakim, 2013; Lindzen, 1981).

1.1.2 Gravity waves in models

The global circulation model (GCM) and chemistry climate model (CCM) have been developed to study the large-scale atmospheric phenomena and those long-term changes. Small-scale gravity waves are generally unresolved in GCM/CCMs because the subgrid-scale phenomena and the gravity wave itself have not been focused in most studies, although the main reason is due to high computational cost. However, without the effect of sub-grid scale gravity waves, it is difficult for such models to reproduce realistic atmosphere. For example, the cold bias in the polar region is known as a common problem in model simulation due to lack of the gravity wave effects (Butchart et al., 2010). It is considered that the resolved wave forcing alone is insufficient to maintain the realistic strength and structure of the polar night

jet. Simulated polar night jet is stronger which is balanced with the colder polar temperature.

To include the gravity wave effect, nearly all global models use gravity wave parameterizations. In past decades, various gravity wave parameterizations have been developed to address the model biases. McFarlane (1987) introduced the orographic gravity wave parameterization which explains the source and breaking/dissipation in the model calculation. In the McFarlane's scheme, the source momentum flux of the gravity wave excited at the surface is determined by the surface wind, atmospheric stability, and complexity of the subgrid-scale topography. This gravity wave instantaneously propagates upward, transferring the momentum to the atmosphere where the wave saturation occurs. The wave saturation proposed by Lindzen (1981) is caused when the amplitude of the wind perturbation associated with the gravity wave exceeds the background mean wind. At this time, the vertical structure of the temperature changes to be unstable because the vertical gradient of the potential temperature is locally inverted ($\partial\theta/\partial z < 0$). The local unstable state is immediately returned to the neutral state ($\partial\theta/\partial z = 0$) so that the amplitude of the perturbation wind reduces to that of the background wind. Associated decrease in the momentum flux is transferred to the atmosphere in the form of the acceleration/deceleration by the wave forcing. Hines (1997) proposed the non-orographic gravity wave parameterization in which the momentum flux of the gravity wave at the source region has a globally uniform distribution.

However, in the real atmosphere neither the source momentum flux of the gravity wave is globally uniform nor the propagation path of the gravity wave is purely vertical, which is different from the assumption used in the gravity wave parameterizations. Sato et al. (2009) showed some properties of gravity waves using a gravity wave resolving high-resolution GCM data. The resolution of their GCM is sufficiently high such that certain gravity wave components, such as excitation, propagation, and breaking are explicitly resolved without gravity wave parameterization (Watanabe et al., 2008; Sato et al., 2009, 2012). They calculated a horizontal distribution of the momentum flux associated with gravity waves in lower

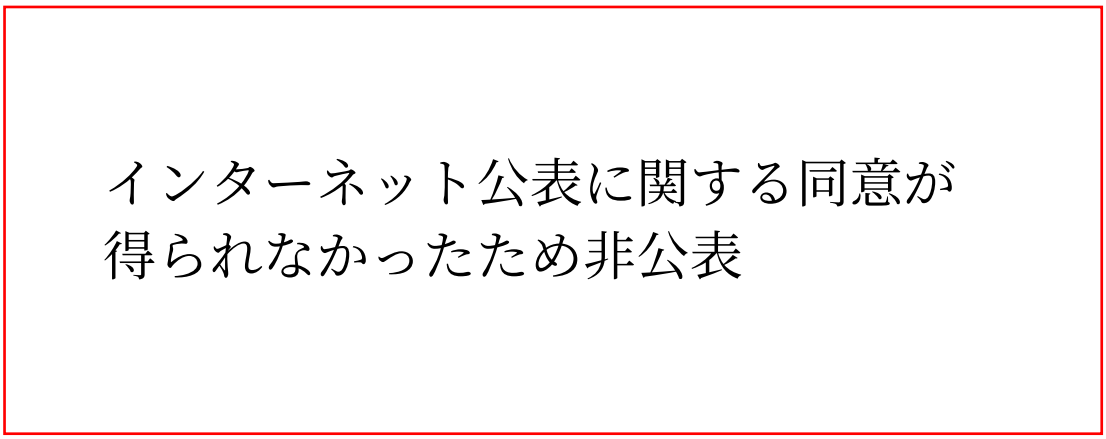

Fig. 1.2 (a) A meridional cross section of momentum flux associated with gravity waves [mPa] (colors) and zonal mean zonal wind [ms^{-1}] (contour) in July simulated by a gravity wave-resolving GCM. (b) Rays of gravity waves (thin curves) in the idealized background westerly winds [ms^{-1}] (contours). Adopted from Sato et al. (2009).

atmosphere. The gravity wave source exhibits longitudinal and latitudinal dependencies. In particular, strong westerly jets, steep mountains such as Andes, and monsoon region are the dominant gravity wave sources. In addition, the meridional cross section of the momentum flux reveals that the gravity waves propagate not only in vertical but also in meridional direction. Figure 1.2a shows the momentum flux associated with the gravity waves (color) and zonal mean zonal wind (contour) in the meridional cross section averaged in July. It is observed that the westward gravity waves generated in the SH high (low) latitudes propagate northward (southward) during the upward propagation. This is confirmed by a simple ray tracing analysis. Figure 1.2b shows rays of gravity waves in the idealized zonal wind distribution. It is found that the rays tend to take paths toward the jet core in both hemispheres, suggesting the latitudinal propagation of the gravity waves.

1.1.3 The residual mean circulation

Lagrangian motion of the mean meridional circulation is approximately expressed by the residual circulation in the transformed Eulerian mean (TEM) framework. The TEM equations are useful to diagnose the wave-mean flow interaction (Andrews and McIntyre, 1976;

Andrews et al., 1987). In the TEM system, the residual velocities $(\overline{v}^*, \overline{w}^*)$ are expressed by sum of the Eulerian mean flow and the Stokes drift:

$$\overline{v}^* = \overline{v} - \frac{1}{\rho_0}\frac{\partial}{\partial z}\left[\rho_0 \frac{\overline{v'\theta'}}{\overline{\theta}_z}\right], \tag{1.1}$$

$$\overline{w}^* = \overline{w} + \frac{1}{a\cos\phi}\frac{\partial}{\partial \phi}\left[\cos\phi \frac{\overline{v'\theta'}}{\overline{\theta}_z}\right], \tag{1.2}$$

where $\overline{v}$ is the zonal mean meridional wind, $\overline{w}$ is the zonal mean vertical wind, ρ_0 is density, θ is potential temperature, a is the radius of the Earth, and ϕ, z are latitude and height, respectively. The overbar $\overline{A}$ and the prime A' denote the zonal mean state of A and the deviation of A from $\overline{A}$, respectively. These velocities satisfy the mass conservation in the meridional cross section:

$$\frac{1}{a\cos\phi}\frac{\partial}{\partial\phi}(\overline{v}^*\cos\phi) + \frac{1}{\rho_0}\frac{\partial}{\partial z}(\rho_0\overline{w}^*) = 0. \tag{1.3}$$

Thus, the stream function Ψ of the residual circulation can be defined as follows:

$$\Psi = -\frac{\cos\phi}{g}\int_p^0 \overline{v}^* dp. \tag{1.4}$$

1.1.4 The role of wave-induced force in the residual mean circulation

The BDC is driven by the forcing associated with breaking/dissipation of the atmospheric waves (Figure 1.1a). A theory frequently used to diagnose the wave-driven general circulation is the "downward control principle" (Haynes et al., 1991). This principle states that the forcing resulting from momentum deposition through the breaking/dissipation of waves that are primarily propagating from the troposphere causes the mean meridional residual flow in the steady state. In the steady state, the zonal momentum equation in the TEM system is written as

$$-\left[f - \frac{1}{a\cos\phi}\frac{\partial(\overline{u}\cos\phi)}{\partial\phi}\right]\overline{v}^* + \frac{\partial\overline{u}}{\partial z}\overline{w}^* = \frac{\nabla\cdot\mathbf{F}}{\rho_0 a\cos\phi} + \overline{X}, \tag{1.5}$$

where $\overline{u}$ is zonal mean zonal wind, f is the Coriolis parameter, and $\overline{X}$ is an unresolved wave forcing term. $\mathbf{F}$ is the E-P flux vector, defined as follows:

$$\mathbf{F} = \rho_0 a \cos\phi \left(\overline{u}_z \frac{\overline{v'\theta'}}{\overline{\theta}_z} - \overline{u'v'}, \left[f - \frac{1}{a\cos\phi} \frac{\partial}{\partial\phi} (\overline{u}\cos\phi) \right] \frac{\overline{v'\theta'}}{\overline{\theta}_z} - \overline{w'u'} \right), \tag{1.6}$$

where θ is the potential temperature. By substituting (1.5) into (1.4), we obtain

$$\Psi_{\mathrm{DC}} = \frac{\cos\phi}{g} \int_p^0 \frac{\mathcal{F}}{\hat{f}} dp, \tag{1.7}$$

where Ψ_{DC} denotes the stream function estimated from the downward control analysis, $\mathcal{F}$ is sum of the forcing terms in the RHS of Equation 1.5, and $\hat{f} = f - \overline{u}_y$. In the steady state, Ψ_{DC} corresponds to Ψ. In addition, the wave forcing term can be linearly decomposed into the different wave components so that the contributions of respective wave forcing to the residual circulation is also linearly extracted from the total circulation.

A quantitative evaluation of the gravity wave effects is necessary and important for understanding of the middle atmosphere dynamics including the BDC. However, this is difficult due to observational and model limitations. An indirect estimation method based on the downward control principle is used to examine the gravity wave effect and BDC in chapter 2.

1.2 Roles of gravity waves in the mean meridional circulation change

The global warming is widely known issue. The middle atmosphere dynamics is expected to be largely affected by the climate change including the greenhouse gas increase and ozone destruction.

1.2.1 BDC trends in the GHG increase

Recent studies using chemistry-climate models (CCMs) show BDC acceleration in terms of changes in lower stratospheric tropical upwelling in response to greenhouse gas (GHG)

increase (Butchart et al., 2000, 2006, 2010; Garcia and Randel, 2008; McLandress and Shepherd, 2009b; Li et al., 2008; Okamoto et al., 2011). It is considered that an increase in the wave forcing in the extratropical lower stratosphere likely causes this acceleration, as expected from theory and confirmed from diagnostic analyses of the model simulations. The BDC acceleration leads to modification of the distribution of ozone and the recovery of the stratospheric ozone. The GHG increase is considered to cause warming of the troposphere and cooling of the middle atmosphere. It is expected that this change will increase the meridional temperature gradient in the subtropical upper troposphere/lower stratosphere because the tropopause is much higher in the tropics than in the extratropics. Associated change occurs in the vertical shear of the zonal wind implying a strengthening of the westerly in the upper part of the subtropical jet (Garcia and Randel, 2008). Several studies have discussed changes in the distribution of wave forcing associated with the zonal wind change and BDC acceleration in the lower stratosphere. Almost all CCM simulations show such response to the GHG increase. In other words, a robust mechanism which changes the wave forcing is that GHG increase pushes the critical layer upward so that the circulation below the forcing is accelerated (Shepherd and McLandress, 2011).

While CCMs consistently predict an increase in tropical upwelling, there is as yet no consensus on a issue, what type of waves is the main driver of the BDC acceleration. Butchart et al. (2006) quantified the contribution of the resolved wave forcing to the upwelling in the models: On average, contribution of resolved wave forcing accounts for 60% of the upwelling and remaining 40% is contributed by parameterized gravity wave forcing. Contribution of orographic gravity wave forcing to the tropical upwelling is studied by Li et al. (2008) and Garcia and Randel (2008), but very different conclusions are suggested in their model simulations. McLandress and Shepherd (2009b) examined the relative roles of planetary waves and synoptic waves as well as stationary and transient waves.

1.2.2 Response to the ozone depletion

The negative trend in column ozone in the Antarctic spring in the last half of the 20th century is a widely known issue (Solomon, 1999). Ozone is largely depleted by chemical reaction with the chlorine that is released when chlorofluorocarbons (CFCs) are destroyed by photolysis or reaction. CFCs have been increasing by anthropogenic sources in the 20th century. The ozone decrease leads to a cooling trend in temperature by the decrease of absorption of solar radiation (Thompson and Solomon, 2002; Randel et al., 2009). These changes affect the mean zonal wind in the stratosphere through the thermal wind balance.

Smith et al. (2010) focused on this point and examined the response in the mesospheric circulation and temperature using the Whole Atmosphere Community Climate Model (WACCM) version 3.5, developed in the National Center for Atmospheric Research (NCAR), which simulates the atmosphere including the lower thermosphere in the last half of the 20th century. They showed a link between the summer polar mesospheric warming trend and stratospheric ozone decrease. The mechanism proposed by Smith et al. (2010) is as follows (Figure 1.3). The westerly trend in the zonal wind in the stratosphere is associated with the negative polar temperature trend due to the ozone loss in the 20th century. The westerly wind trend tends to prevent upward propagation of gravity waves having eastward phase velocities. Thus, the net convergence of the momentum flux associated with gravity waves in the mesosphere is shifted toward easterly acceleration leading to a deceleration of the mesospheric equatorward flow in summer. As a result, weakening trends of the upwelling in the mesosphere and of the downwelling in the lower thermosphere occur in the polar region. The vertical flow trend results in a temperature trend; warming in the mesosphere and cooling in the lower thermosphere. The warming mesospheric temperature trend is not seen in an additional experiment of “fixed halogen” run, in which the surface abundances of halogen compounds are held fixed at 1960 levels, producing no ozone hole in the late

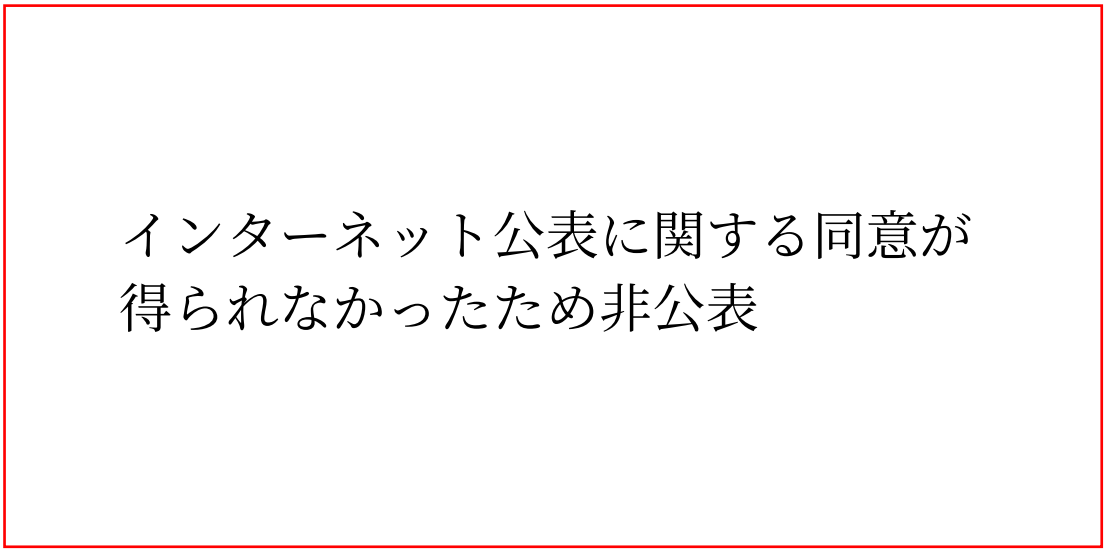

Fig. 1.3 Linear trends in (a) temperature (units: $\mathrm{K/47years}$; contour intervals 4), (b) zonal wind (units: $\mathrm{m/s/47years}$; contour intervals 4), (c) gravity wave drag (units: $\mathrm{m/s/day/47years}$; contour intervals 8), (d) residual mean meridional flow (units: $\mathrm{m/s/47years}$; contour intervals 0.4), and (e) residual mean vertical flow (units: $\mathrm{cm/s/47years}$; contour intervals 0.2) over the period 1960-2006 averaged over the months of November and December. Negative contours are dashed and zero contours are not drawn. Adopted from Smith et al. (2010).

20th century. This result is consistent with the above scenario. They also suggested that the observational evidence for the hemispheric asymmetries in the polar mesospheric cloud (PMC) and the related dynamics (e.g. Bailey et al., 2007; Xu et al., 2007) is the consequence of the hemispheric asymmetry in the polar ozone.

The summer stratosphere-mesosphere vertical coupling has also been shown by several studies using other model data or observations (e.g. Lossow et al., 2012; Benze et al., 2012). Benze et al. (2012) showed the correlated relation between the onset of the PMC season and the reversal date of the stratospheric zonal wind using data from the Solar Backscatter Ultraviolet (SBUV) satellite instrument. It was found that the timing of the shift from winter to summer in the SH stratospheric zonal wind controls the timing of the onset of PMC seasons. The stratospheric zonal wind is closely related to the mesospheric dynamics.

In contrast, it is expected that the SH polar ozone recovers the 1960's level by the late 21st

century, while GHG continuously increases. Now we are interested in how the stratosphere-mesosphere coupling proposed by Smith et al. (2010) works in a period of both ozone and GHG increase. In chapter 3, WACCM data is used to examine the mean meridional circulation change and roles of atmospheric waves in the climate change.

1.2.3 Remote interaction in the middle atmosphere

The semiannual oscillation (SAO) in the temperature variations in the tropical stratopause was first discovered by Reed (1962) and is mainly driven by atmospheric waves, while momentum advection is also an important factor for the SAO phases (Peña-Ortiz et al., 2010). For example, it has been discussed previously that the westerly phase of the SAO is driven by fast Kelvin waves and that the easterly phase is driven by upward-propagating gravity waves and/or planetary waves propagating from the mid-latitudes of the winter hemisphere (e.g., Hirota, 1978, 1980; Dunkerton, 1979; Garcia et al., 1997). The momentum advection from the summer hemisphere is related to the middle-atmosphere Hadley circulation (Dunkerton, 1989; Peña-Ortiz et al., 2010). Another well-known equatorial oscillation is the quasi-biennial oscillation (QBO) in the lower stratosphere (Baldwin et al., 2001). The alternating downward propagation of the easterly and westerly QBO shear zones is driven by the westward and eastward gravity waves, as well as by Kelvin waves (Sato and Dunkerton, 1997). The QBO and SAO are closely related because they are both influenced by wave-mean flow interaction. Upward propagation of gravity waves is modulated by the filtering depending on the QBO phases (e.g., Dunkerton and Delisi, 1997). In addition, it is also known that the QBO affects the extratropical dynamics (Holton and Tan, 1980, 1982). Planetary waves tend to propagate into the polar region when the QBO phase is easterly, leading to a weakening of the PNJ due to easterly momentum deposition. As noted above, the QBO effect on the winter hemispheric dynamics has been well studied. On the other hand, discussions of the relation between the SAO and winter hemisphere seem to be not sufficient. In the present study,

the effect of the interannual SAO variation on the winter hemispheric dynamics is examined within the TEM framework.

Hitchman and Leovy (1986) investigated relations between the SAO and residual circulation using temperature data obtained from the Limb Infrared Monitor of the Stratosphere (LIMS) experiment. In their analysis, the residual mean meridional flow around the SAO levels is maximized beneath the descending zero wind line. That level also corresponds to the maximum penetration of the easterly wind into the winter hemisphere. Additionally, the existence of rising motion in the subtropical lower mesosphere of the northern hemisphere (NH) was shown. They also showed that the subtropical ascent pattern descends with the SAO over the equator, a phenomenon they attributed to wave-mean flow interaction in the subtropics near the SAO easterly phase levels. In the present thesis, this point is examined in detail using a high-resolution GCM and long-term reanalysis data, and is discussed in terms of the possibility of an upwelling controlled by the SAO variations.

One of the remaining topic in the remote connection is a possible dynamical connection between the winter pole and the equator in the upper stratosphere/lower mesosphere that indicates a coupling of the SAO and the PNJ. Since planetary waves and gravity waves significantly influence both the easterly phase of the SAO and the PNJ, it may not be surprising that the SAO and PNJ have some kind of connection via planetary waves and gravity waves. In this thesis, austral winter is focused because the SAO-PNJ interaction in the SH is clearly observed, while analysis for boreal winter is difficult and beyond the scope because interannual variability of the PNJ is too large so that the SAO-PNJ interaction is unclear in the NH. This third topic is examined in chapter 4, and considered to be an extension of the study discussed in chapter 2.

1.3 Purpose of this study

As stated above, several interesting issues on the residual mean circulation and roles of atmospheric waves in the middle atmosphere are remaining and should be addressed. Purposes of this study are to understand the following topics;

- roles of gravity waves on the structure, strength, and seasonal variation of the BDC,
- response of the upper stratosphere, mesosphere, and lower thermosphere to the ozone increase and greenhouse gas increase,
- possible dynamical connection between SAO variation and PNJ variation, related to wave forcing and the residual mean circulation.

This thesis is organized as below. In chapter 2, the wave contributions to the BDC are examined using a reanalysis data set. The reanalysis data includes gravity wave effects in the mean state by the assimilations of the observational data. Thus, certain part of the gravity wave effect can be estimated from the downward control principle. This method is applied to several reanalysis data sets to demonstrate roles of the gravity waves in the stratospheric circulation. In chapter 3, dynamical responses in the middle atmosphere is investigated using WACCM data which simulated the future climate change. Future changes in the middle atmosphere simulated by WACCM includes both the responses to the ozone recovery and greenhouse gas change. In this analysis, effects of ozone trend and greenhouse gas trend are separately examined. The former is performed as a confirmation of the mechanism proposed by Smith et al. (2010). In particular, response in the propagation of the gravity waves to the change in the stratospheric wind distribution is examined in detail. In chapter 4, the SAO variation and related dynamics for austral winter are examined using gravity wave resolving GCM data and a reanalysis data. In the first half of this chapter, seasonal variation of the zonal wind, residual circulation, and wave forcing in austral winter is shown. Then, the SAO-

PNJ relation is examined by statistical analyses from long-term reanalysis data. Concluding remarks are given in chapter 5.

In this thesis, different data will be used for different purposes in each chapter. In chapter 2, the ERA-Interim data is used to investigate the mean state of the BDC and wave roles on it. The ERA-Interim is considered to be one of the latest and most reliable reanalysis data which has been widely used in many fields. It is known that the stratospheric circulation was improved to be more realistic than that of ERA-40, the old version of the ERA-Interim. In contrast, we will study effects of the CO_2 and ozone trends on the BDC in future climate in chapter 3. To examine the future climate, model simulation data has to be used. In addition, the results for the future climate including the ozone increase scenario should be compared with those for the past climate of Smith et al. (2010). The WACCM data was analyzed by Smith et al. (2010) and WACCM has recently been integrated to the end of 21st century with ozone increase scenario and regulated CO_2 scenarios. For these reasons, we examine the middle atmosphere dynamics in the future climate using the WACCM simulation data. In chapter 4, the stratospheric seasonal evolution and links of the polar and equatorial dynamics in it are examined in detail. Since the PNJ and the equatorial SAO are the main focus of this chapter, the analysis range includes not only the stratosphere but also the lower mesosphere. The dynamics of atmospheric waves including the gravity wave is also important as a factor controlling the SAO and PNJ variations. In this chapter, a gravity wave-resolving GCM data extending to the upper mesosphere is used. The GCM well resolves the atmospheric waves of broad range (horizontal wavenumber < 213), which is considered to be sufficient to reproduce the realistic atmosphere. However, only a few years for the GCM analysis are available, which gives a case study of the seasonal variation. Long-term reanalysis data is useful to examine the GCM results. To be able to compare the results with the GCM, we should use the high-top reanalysis/model simulation data including the mesosphere. The MERRA data is used in this chapter since it is one of the highest-top reanalysis data extending

to the lower mesosphere.

Chapter 2

Roles of atmospheric waves on the Brewer-Dobson circulation

The stratospheric circulation is in general dominated by large-scale waves such as the Rossby waves. The planetary waves propagate into deep winter stratosphere and drive a deep branch of the BDC, while the synoptic-scale waves drive the poleward flow associated with the shallow branches in both hemispheres. Such global circulation and large-scale waves are well resolved in GCMs and investigated. On the other hand, recent studies have been focusing on the importance of the gravity waves in the stratosphere (Butchart et al., 2006, 2010; Li et al., 2008; Garcia and Randel, 2008; McLandress and Shepherd, 2009b; Okamoto et al., 2011). However, the treatments of the gravity waves in GCMs are not realistic because the determination of the several parameters for the gravity waves cannot be limited by the observations. In contrast to GCMs, the reanalysis data involves “realistic” effects of the gravity waves in the mean fields by assimilation scheme using the observational data. Therefore some part of the gravity wave effects can be extracted from the mean field of the reanalysis data. In this chapter, a diagnostic estimation method for the gravity waves in the reanalysis data is introduced and applied to analyses on the BDC.

The purpose of this chapter is to examine the importance of the gravity waves on the BDC from a reanalysis data. The content of this chapter is as follows. Brief descriptions of the

reanalysis data are given in section 2.1. In section 2.2, diagnostic estimation method of the gravity wave contribution to the BDC is introduced based on a TEM system. Roles of gravity waves on several aspects of the BDC are examined using the diagnostic estimation method and the results are described in section 2.3. A summary for this chapter is given in section 2.4.

2.1 Data description

ERA-Interim (Dee et al., 2011) is the latest version of the ERA-40 reanalysis data (Uppala et al., 2005) produced by the European Centre for Medium-Range Weather Forecasts (ECMWF). The ERA-Interim reanalysis data covers years from 1979 to the present days including multiple observational datasets; conventional observations such as radiosondes and wind profilers; observations by satellite instruments such as MSU and SBUV; observations from buoys; and etc. are used. The major update from the ERA-40 is the use of 4D-Var assimilation schemes. The 4D-Var makes more effective use of observations. Moreover, inclusion of the variational bias correction scheme to reduce systematic differences among satellite observations led to the consistent vertical profile of the temperature (Dee and Uppala, 2008). The ERA-Interim significantly improved the representation of the stratospheric circulation over the ERA-40. The BDC largely influences the mean age of air, which is the residence time of the air parcel in the stratosphere. The distribution of the age of air in the lower stratosphere for the ERA-Interim is consistent with observations, which is longer than that in the ERA-40. Dee et al. (2011) also reported that the vertical distribution ozone in the lower stratosphere is improved over the ERA-40. The resolution of the output data used in this study is $1.5^\circ \times 1.5^\circ$ with 37 vertical levels from the surface to 1 hPa. In this study, we mainly examine the wave effects on the climatology and seasonal variation of the BDC for the period of 1990-2002.

Results from the ERA-Interim are compared and validated by those from recent reanalysis

data sets such as the National Centers for Environmental Prediction (NCEP)-Climate Forecast System Reanalysis (CFSR) (Saha et al., 2010), Modern Era Retrospective-analysis for Research and Applications (MERRA) (Rienecker et al., 2011), JRA-55 (Kobayashi et al., 2015), but they are not shown in this thesis.

Figure 2.1a shows a climatology of zonal mean zonal wind (contour) and zonal mean temperature (color) in meridional cross section averaged for July in 1990-2002 for the ERA-Interim data. Subtropical jets are located around 200 hPa at 30°S and 40°N with maximum wind speeds of 40 and 20 ms^{-1}, respectively. In the stratosphere, the westerly shear of the polar night jet is balanced with strong positive temperature gradient in high latitudes of the Southern Hemisphere (SH). On the other hand, easterly wind is dominant in the summer stratosphere but the westerly wind intrudes up into the 20 km altitude in the lower stratosphere in the mid-latitudes and polar region. The stream function of the residual circulation averaged for July in 1990-2002 is shown in Figure 2.1b. The stream function is composed of negative circulation and positive circulation. The former is the deep branch centered in the SH extending to high altitudes and to the Northern Hemisphere (NH). The extension of the deep branch to the NH did not appear in the schematic illustration by Plumb (2002) (Figure 1.1a), but this feature is generally observed for the solstice seasons in almost all the data including observational, reanalysis, and model data, which is examined in the following section in detail. The latter is the shallow branch located in the NH limited to lower stratosphere. The negative circulation dominates over the positive circulation in the stratosphere. These are the common features in other reanalysis data sets with minor differences in magnitude and shape (not shown).

2.2 Indirect estimation method of GW contribution

The residual mean circulation is driven by the wave forcing. In this section, the downward control (DC) analysis (Haynes et al., 1991) is used to evaluate the contribution of the gravity

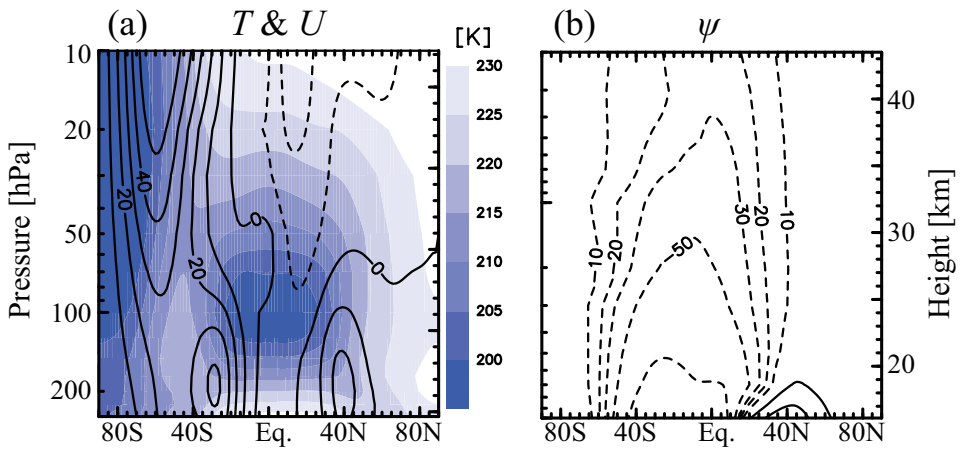

Fig. 2.1 Meridional cross sections of (a) zonal mean zonal wind (contour) and zonal mean temperature, and (b) the stream function of the residual mean circulation averaged for July in 1990-2002 calculated from ERA-Interim data. Contour interval is 10 ms^{-1} for (a).

wave forcing to the residual mean circulation.

2.2.1 GW contribution to the residual mean circulation

Due to limitation of data availability for the gravity wave forcing in the reanalysis data sets, the GW contribution is not explicitly calculated. Instead, the GW contribution is indirectly evaluated as the difference between the stream function and the contribution of the resolved wave forcing. Since the forcing term $\mathcal{F}$ in Equation 1.7 is linearly separable, the contribution of the resolved wave forcing to the stream function is evaluated as

$$\Psi_{\mathrm{EPFD}} = \frac{\cos\phi}{g}\int_p^0 \frac{\mathrm{EPFD}}{\hat{f}}dp, \tag{2.1}$$

where EPFD is the E-P flux divergence (the first term of the RHS of Equation 1.5). Because in the steady state the residual mean circulation is driven by the large-scale wave forcing and the small-scale wave forcing, the contribution of gravity waves is estimated using Equations 1.4, 1.7, and 2.1 as follows:

$$\Psi_{\mathrm{GWD}^\dagger} = \Psi - \Psi_{\mathrm{EPFD}}, \tag{2.2}$$

where † means indirectly estimated value. The residual $\Psi_{\mathrm{GWD}^\dagger}$ theoretically corresponds to the contribution of unresolved scale waves in the steady state. In the reanalysis data, $\Psi_{\mathrm{GWD}^\dagger}$ does not express only the unresolved wave contribution because the reanalysis data includes the analysis error associated with the assimilation. However, this method is sufficiently useful to evaluate the unresolved wave effects when the large-scale fields are well reproduced for a following reason. In the TEM system, the zonal mean zonal equation in the steady assumption states that the residual circulation is equal to the E-P flux divergence ($-\hat{f}\overline{v}^* \sim \mathrm{EPFD}$). The residual mean meridional flow $\overline{v}^*$ consists of mean (ageostrophic) velocity $\overline{v}$ and the Stokes drift $\overline{v}^s$. In the TEM zonal momentum equation, the Stokes drift in the LHS is canceled by the term relating the heat flux in the EPFD of the RHS (see Equations 1.5 and 1.6). Thus, it turns out that the mean meridional wind is driven by the momentum flux divergence. In the stratosphere, the heat flux is mainly attributed to the Rossby waves and the momentum fluxes are driven by the Rossby waves and gravity waves. Therefore, if the large-scale mean wind is well reproduced by the data assimilation, certain part of gravity wave effects are included there and estimated as a difference of the mean wind and the momentum flux divergence associated with the large-scale waves, which is consistent with Equation 2.2. This assumption is well considered by Okamoto et al. (2011). Okamoto et al. (2011) compared the indirectly-estimated gravity wave contribution with the parametrized gravity wave contribution using a CCM data, which suggested that both gravity wave effects show little difference in the middle atmosphere indicating one of the evidences for the validity of this method. Thus in this study, a field obtained by subtracting the resolved wave contribution from the residual mean circulation is called the “GW contribution” including all effects other than the resolved wave contribution.

2.2.2 GW contribution to the tropical upward mass flux

The mass stream function averaged on a pressure surface is called the mass flux (Holton, 1990) defined by

$$F(p) = 2\pi\rho_0 a^2 \int_{\phi_1}^{\phi_2} \overline{w}^* \cos\phi d\phi \tag{2.3}$$

where ϕ_1 and ϕ_2 are specific latitudes. Since the BDC is two-celled in the lower stratosphere, total upward mass flux is estimated when ϕ_1 and ϕ_2 correspond to the turnaround latitudes where $\overline{w}^* = 0$ for SH and NH, respectively. From the mass conservation, $\overline{w}^*$ is expressed by the meridional integration of the stream function Ψ. Thus, Equation 2.3 is rewritten as

$$F(p) = 2\pi a \left[\Psi(\phi_2) - \Psi(\phi_1)\right]. \tag{2.4}$$

Because the stream function can be linearly separated into different wave contributions as above, the GW contribution to the total mass flux is indirectly calculated by

$$F_{\mathrm{GWD}^\dagger} = F - F_{\mathrm{EPFD}} \tag{2.5}$$

where $F_{\mathrm{EPFD}} = 2\pi a[\Psi_{\mathrm{EPFD}}(\phi_2) - \Psi_{\mathrm{EPFD}}(\phi_1)]$.

2.3 Results

In this section, we investigate several aspects of GW contributions to the BDC in the lower and mid-stratosphere using the diagnostic method. First, GW role in the formation of the summer subtropical upwelling of the BDC is shown from a viewpoint of the stream function of the residual circulation. Second, magnitude of GW contribution to the strength of the BDC in the lower stratosphere is compared to contribution of the resolved wave. Next, GW importance in the structure of the BDC is examined in terms of the turnaround latitudes in the lower stratosphere. Finally, GW and PW contributions to the seasonal variation of the BDC is shown, particularly focusing on differences between the lower stratosphere and mid-stratosphere.

2.3.1 GW contribution to the formation of the BDC

Figure 2.2 shows meridional cross sections of the residual circulation, resolved wave contribution estimated from Equation 2.1, and GW contribution estimated from Equation 2.2 for January and July in ERA-Interim data. The residual mean circulation is composed of two cells, a large winter cell and a small summer cell. Both cells have upwelling in the lower latitudes and downwelling in the extratropics associated with the poleward mass transport. The winter cell extends to higher altitudes and the summer hemisphere. On the other hand, the summer cell is shallow and weaker than the winter cell and limited to the mid- and high latitudes.

In the steady state, the DC theory indicates the wave-driven circulation. The residual mean circulation is mainly explained by the resolved wave contribution. The stream function in the winter stratosphere and the summer lower stratosphere is dominated by the resolved wave contribution for both seasons. In particular, the stream function induced by the EPFD has large vertical variation in the extratropics suggesting that the large meridional flow is driven by the EPFD. These features are consistent with previous studies which showed that the deep branch in the winter hemisphere is driven by the planetary waves and the shallow branches in both hemispheres are driven by the synoptic-scale waves (e.g., Figure 1.1a). However, the upwelling in the subtropics in the summer hemisphere and the poleward flow in the mid-latitudes in the lower stratosphere is not driven only by the resolved wave contribution.

The residual is considered to be the “GW contribution” in this study. Right panels of Figure 2.2 indicate that the upwelling in the summer subtropics in the whole stratosphere is mainly driven by the GWs. Moreover, poleward flow in the low and mid-latitudes in the winter hemisphere in the lower stratosphere is also driven by GWs. These results are consistent with the previous studies (Okamoto et al., 2011).

In addition, a weak deep branch of the summer circulation is observed especially in the NH

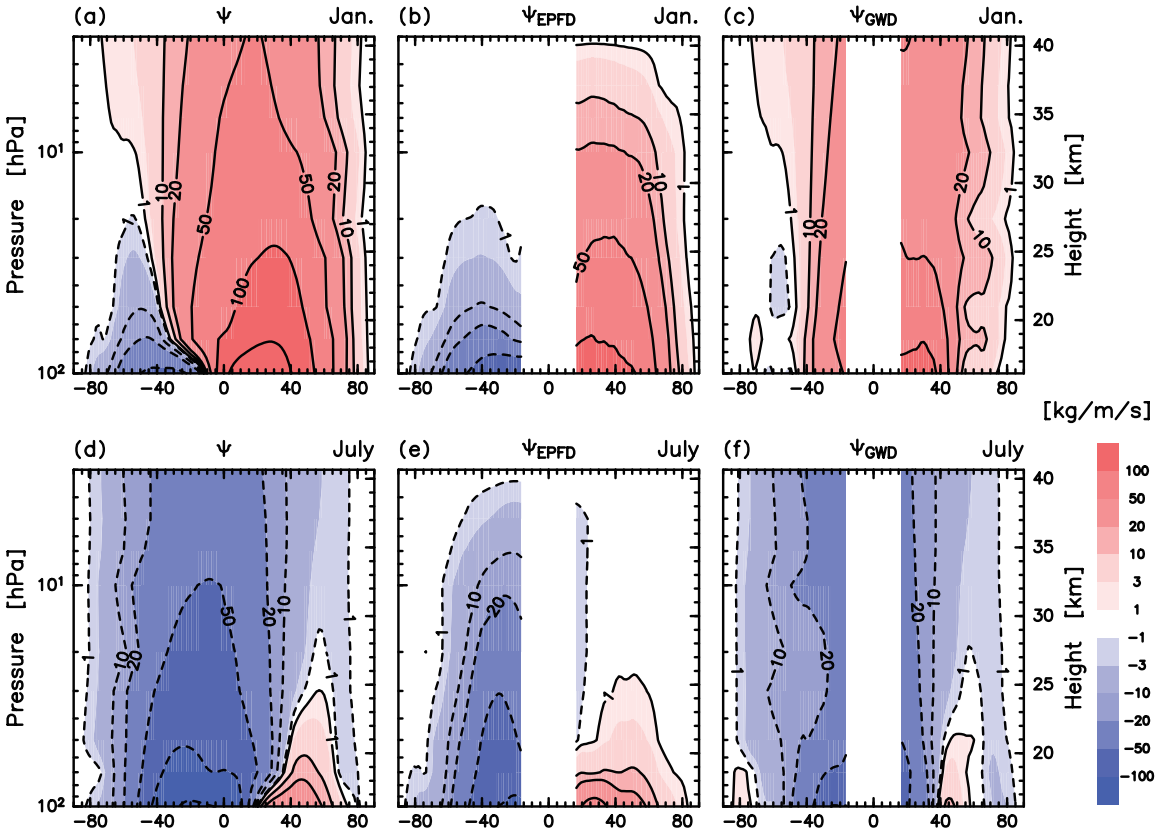

Fig. 2.2 Meridional cross sections of (left panels) the stream function of the residual circulation, and contributions of (center panels) resolved wave forcing and (right panels) gravity wave forcing as a residual, for (upper panels) January and (lower panels) July calculated from the ERA-Interim data.

in July. This is not explained by the resolved wave contribution but by the GW contribution. This is because the summer stratosphere is generally dominated by the easterly wind (Figure 2.1a) so that the propagation of the planetary waves into the deep stratosphere is prevented. It is considered that the eastward GW momentum flux convergence occurs in the mid- and upper stratosphere in the summer hemisphere and drives the summer-poleward flow there.

Sato et al. (2009) suggested that GWs are generated in the Asian monsoon region in the summer subtropics, which can propagate into the upper stratosphere and break to drive the equatorward flow followed by the strong upwelling in the summer subtropical stratosphere. The GWs inducing poleward flow in the winter lower stratosphere is considered to be oro-

graphic GWs which tend to break above the subtropical jet (Li et al., 2008; McLandress and Shepherd, 2009b; Okamoto et al., 2011; Shepherd and McLandress, 2011).

All these features are consistent with results obtained from other reanalysis data sets (not shown). Thus, the GW is important as a driver of the BDC particularly for the extension of the winter circulation into the summer hemisphere and poleward flow in the mid-latitudes in the lower stratosphere.

2.3.2 GW contribution to the strength of the BDC

As mentioned above, the GW contribution is not negligible even in the lower stratosphere. In this section, the GW contribution to the strength of the BDC is qualitatively investigated using the tropical upward mass flux calculated from Equations 2.4 and 2.5.

Green bars in Figure 2.3a show the upward mass flux at 70 hPa averaged for the period of 1990-2002 for the ERA-Interim data. The annual mean tropical upward mass flux is about 6.5×10^{9} [kg s^{-1}]. Contributions by resolved waves and GWs are plotted by blue and red bars, respectively. The resolved wave contribution is about 4×10^{9} [kg s^{-1}]). This value is similar to those calculated from other reanalysis data sets (not shown). This result indicates that the resolved waves at this level are dominated by the large-scale waves such as planetary waves and synoptic-scale waves which are well resolved by most models: the EPFD contribution is over 70% of the total mass flux.

The residual is considered to be mostly driven by the GWs (about 30% contribution to the total mass flux). In other words, GWs may be an important factor for the strength of the BDC even in the lower stratosphere. This fact is consistent with the results in Figure 2.2: At 70 hPa level, the GW contribution to the stream function of the residual circulation is comparable to resolved wave contribution particularly in the mid-latitudes. As mentioned above (Equation 2.4), the upward mass flux is defined by the stream function at a turnaround latitude and the turnaround latitude is located in the mid-latitudes at 70 hPa. Thus, the GW contribution

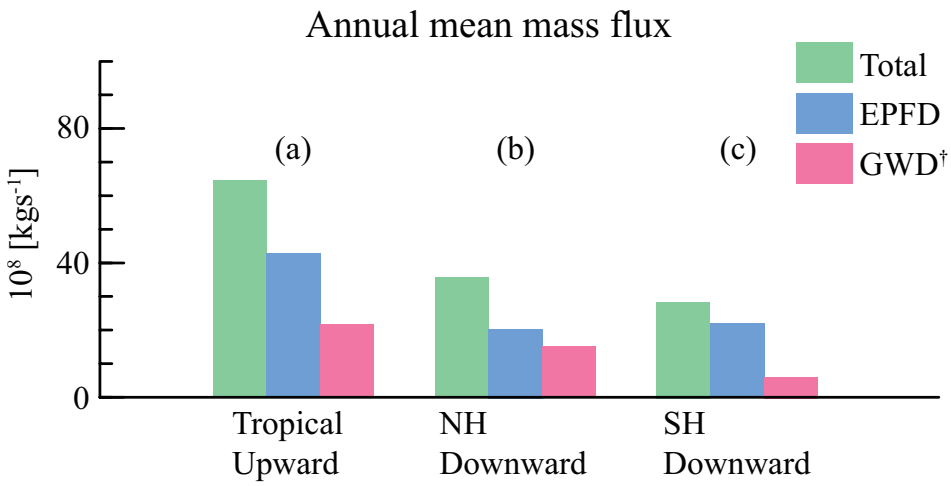

Fig. 2.3 (a) Annual mean tropical upward mass flux at 70 hPa (green) and contributions of the resolved wave forcing (blue) and gravity wave forcing (red) for the ERA-Interim data. NH and SH components are plotted in (b) and (c), respectively.

to the mass flux can be large even in the lower stratosphere. Note that, in contrast to the EPFD contribution, the GW contribution among the models has the variability from 2×10^9 to 4×10^9 [kg s^{-1}], corresponding to the variability from 30% to 50% contribution to the total mass flux (not shown). This difference among models is interesting and should be examined, but is beyond the scope of this thesis.

From Equation 2.4, the mass flux can be decomposed into the NH and SH components, namely downward mass fluxes in the respective hemisphere. The results are shown in Figures 2.3b and 2.3c. The total mass flux is larger in the NH than in the SH. The hemispheric difference mainly comes from the difference in the GW contribution at 70 hPa. In the SH, the resolved wave contribution accounts for about 90% of the total mass flux, but GW and resolved wave contributions are comparable in the NH. The reason for the hemispheric difference is considered as follows. In the SH lower stratosphere, the westerly wind tends to remain even in the early summer so that the planetary waves can propagate there, while almost all the polar night jet breaks within spring season to prevent the long-term intrusion of the planetary waves in the NH lower stratosphere in the ERA-Interim data (not shown).

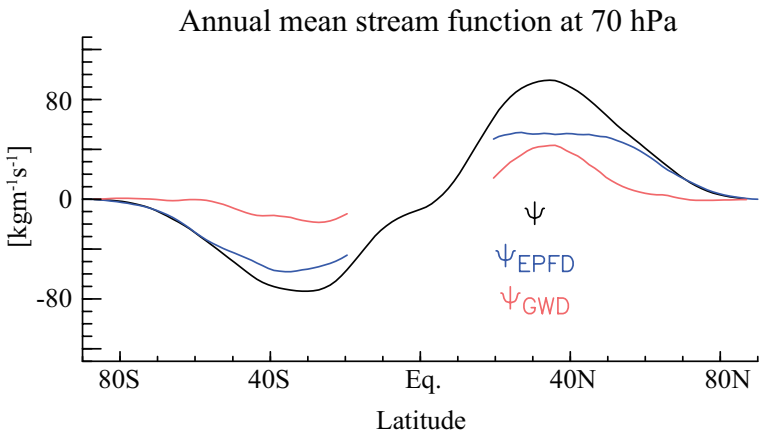

Fig. 2.4 The stream function of the residual circulation at 70 hPa (black curves) and contributions of the resolved wave forcing (blue) and gravity wave forcing (red) are plotted as a function of latitude for the the ERA-Interim data.

Thus, the annually averaged SH EPFD contribution is comparable to the NH one although the winter-time planetary wave activity for the NH is stronger than for the SH. In addition, the GW contribution is large in the NH than in the SH at this height. This may be related to the hemispheric difference in the orographic GWs due to the topographical difference.

2.3.3 GW contribution to the structure of the BDC

The previous subsection describes importance of the GWs to the strength of the BDC in the lower stratosphere, which is related to the location of the turnaround latitudes. Thus, in this subsection, we examine what determines the turnaround latitude in terms of wave contribution. The turnaround latitude is defined as a latitude where the vertical flow $\overline{w}^*$ changes its sign (i.e. upward in the lower latitudes and downward in the higher latitudes). In other word, the turnaround latitudes correspond to the latitudes where the stream function of the residual circulation takes its maximum and minimum. Figure 2.4 shows latitudinal profiles of the annual mean stream function at 70 hPa, and contributions of resolved waves (blue) and gravity waves (red) for the ERA-Interim data. The turnaround latitudes are located at around 30° in both hemispheres.

The resolved wave contribution globally predominates over the GW contribution except for the mid-latitudes in the NH. Thus, the magnitude of the global stream function mainly contributed by the resolved waves. However, focusing on the determination of the turnaround latitude, the resolved wave-induced stream function is flat around the turnaround latitude in both hemispheres and does not have a sharp maximum or minimum. Instead, the GW-contributed stream function tends to form the maximum and minimum around the turnaround latitudes, particularly in the NH. These structures of the EPFD and GW contributions are caused because the resolved wave forcing distribution is broad in the low and middle stratosphere, while the GW forcing in the low and middle stratosphere is limited to the region above the subtropical jet leading to the maximum in the stream function there.

Contributions of the GWs in each hemisphere have large contrast. Near the turnaround latitudes, the magnitude of GW-induced stream function in the NH is larger than that in the SH. This fact is consistent with the results from Figures 2.3b and 2.3c. The results suggest that GWs at this level in the NH mid-latitudes deposit more momentum than in the SH mid-latitudes.

As noted by many previous studies, the upward mass flux is dominated by the downward mass flux in the winter hemisphere (Okamoto et al., 2011; McLandress and Shepherd, 2009b). The downward mass flux is also larger in the winter hemisphere than in the summer hemisphere in this study (not shown). Moreover, the maximum/minimum of the GW-induced stream function mainly determines to the maximum/minimum of the stream function in the winter hemisphere, also suggesting the importance of the GWs in the lower stratosphere. These results are consistent in all other reanalysis data sets (not shown).

2.3.4 GW contribution to the seasonal variation of the BDC

Finally, respective wave contributions to the seasonal variation of the BDC are examined. As is shown, the seasonal variation of the mass flux depends on the height for which the

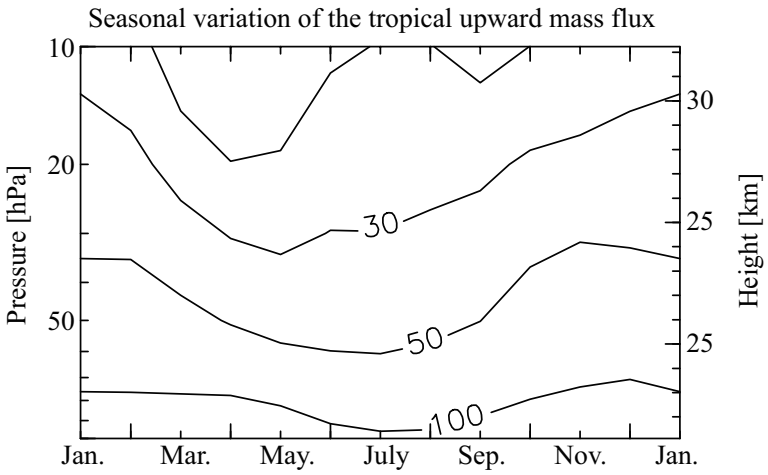

Fig. 2.5 Time-height cross section of the total tropical upward mass flux for the ERA-Interim data. Contours are for 20, 30, 50, and 100 kgs^{-1}.

mechanism is discussed.

Time-height cross section of the monthly-mean upward mass flux for the ERA-Interim data is shown in Figure 2.5. In the lower stratosphere below 50 hPa, the mass flux shows annual variation that has a maximum in boreal winter and a minimum in boreal summer. On the other hand, the mass flux seems to show semi-annual variation in higher altitudes with maxima in solstices and minima in equinoxes. These features are observed in all other reanalysis data sets. To examine this difference between the two height regions, the mass flux is decomposed into the NH and SH contributions.

Figure 2.6a shows seasonal cycles of the total mass flux, NH contribution, and SH contribution at 70 hPa for the ERA-Interim data. Total upward mass flux has an annual cycle with a maximum in boreal winter and a minimum in boreal summer. This seasonal variation is approximately determined by the NH component. The NH component has a maximum in December corresponding to the total mass flux. A minimum of the NH component is in June which is 1-2 months earlier than that of the total mass flux. The NH component has the annual average of 4×10^9 kgs^{-1} and amplitude of 4×10^9 kgs^{-1}. On the other hand, seasonal variation of the SH component shows nearly anti-correlation with the total mass flux

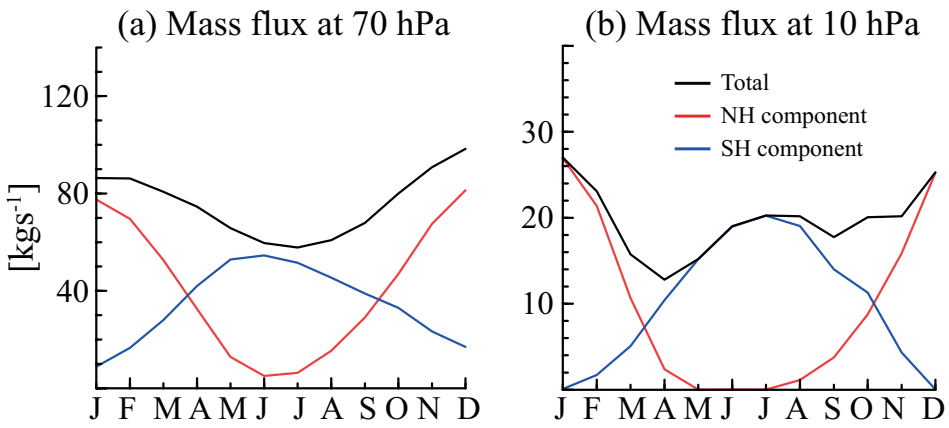

Fig. 2.6 Time series of monthly-mean total upward mass flux (black curves), NH component (red curves), and SH component averaged for the period of 1990-2002 at (a) 70 hPa and (b) 10 hPa.

and the NH component with a maximum in June and a minimum in January. Annual average and amplitude of the seasonal variation of the SH component are smaller than those of the NH component. Thus, the total mass flux as a sum of the NH and SH components exhibits annual variation dominated by the NH variation.

At 70 hPa, the magnitude of the stream function is mainly contributed by the resolved wave component as seen in Figure 2.4. Note that the GWs are important for the determination of the turnaround latitudes. Thus, the large-scale waves are one of the key factors for the seasonal variation of the mass flux at 70 hPa. In general, the activity of planetary waves is lager in NH winter than that in SH winter. This fact may control the difference in the amplitude of time variation of the mass flux. Moreover, the minimum of SH component is larger than that of NH component. This is probably because the westerly wind in the SH lower stratosphere tends to remain through spring so that the planetary waves propagate into the lower stratosphere. This is also important to enlarge the maximum in boreal winter in the total mass flux.

Next, the mechanism of semiannual variation of the mass flux in the middle stratosphere is investigated. Time series of the total mass flux, NH component, and SH component at 10 hPa is shown in Figure 2.6b. As in Figure 2.5, the total mass flux exhibits a semiannual cycle

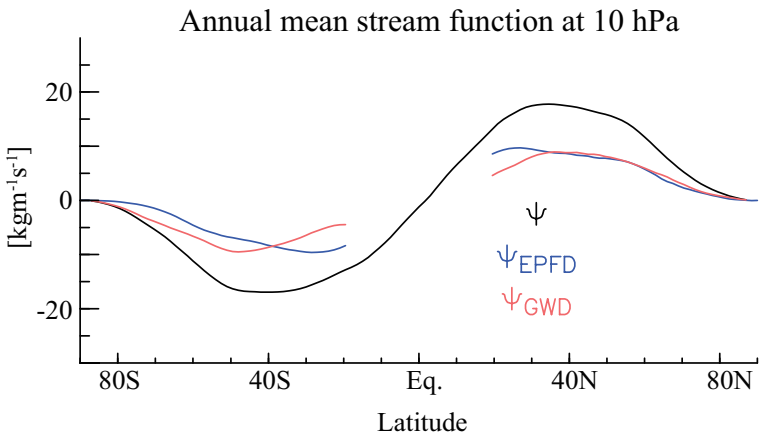

Fig. 2.7 The stream function of the residual circulation at 10 hPa (black curves) and contributions of the resolved wave forcing (blue) and gravity wave forcing (red) are plotted as functions of latitude for ERA-Interim data.

with maxima in solstices and minima in equinoxes. The time variations of the NH and SH components are antiphase, which is similar to those in the lower stratosphere. However, the amplitudes of variations of the NH and SH components are comparable at this height. Note that the vertical scale is different from Figure 2.6a. Thus, the sum of these components shows a semiannual variation. The amplitude for the first cycle tends to be larger than that for the second cycle, because the minimum of the NH component (June) is observed slightly earlier than the maximum of the SH component (June-August) and because the NH component change is faster in January to June than in June to December. This difference between the first and second cycles should be investigated in future. One possible reason is considered that the zonal wind in the NH middle stratosphere drastically changes its sign in late winter/early spring due to the large amplitude planetary waves, which affects the gravity and planetary wave propagations from the lower stratosphere to the middle and upper stratosphere.

Similar to the discussion for Figures 2.3 and 2.4, the contributions of different waves to the seasonal variation of the mass flux at 10 hPa should be examined. The annual mean stream function at 10 hPa, and contributions of resolved waves and GWs for the ERA-Interim data are shown as a function of the latitude in Figure 2.7. At this height, the GW contribution is

comparable to the EPFD contribution. Thus, influence of the interhemispheric difference in the planetary wave activity can be smaller at 10 hPa than at 70 hPa. In addition, the interhemispheric difference in the GW contribution is also smaller (Figure 2.4). These less differences in the amplitudes of NH and SH component result in dominance of the semiannual variation. Note that results from other reanalysis data sets are consistent (not shown), suggesting the general feature of the stratospheric waves and the seasonal variation of the BDC.

2.4 Summary

In this chapter, the climatology of the structure and seasonal variation of the BDC are examined using the ERA-Interim reanalysis data focusing on the wave-driven residual mean circulation in the steady state. The GW contribution to the BDC is defined by the indirect estimation method (Equation 2.2). The resolved waves such as Rossby waves drive the deep branch of the BDC in the winter hemisphere and shallow branches in both hemispheres, while the GW contribution affects the summer tropical upwelling and the shallow branch in the winter hemisphere (Figure 2.2). The GW contribution is also important for the tropical upward mass flux in the lower stratosphere, especially in the NH component (Figure 2.3). In addition, the GW contribution to the stream function of the residual mean circulation in the lower stratosphere has a sharp maximum in the NH mid-latitude suggesting the importance of the GWs on the formation of the turnaround latitude, although contribution to the global average is smaller than the contribution of the resolved waves. The seasonal variation of the tropical mass flux depends on the altitude showing annual cycle in the lower stratosphere and semiannual cycle in the mid-stratosphere. This is mainly caused by the hemispheric difference in the GW and EPFD contributions. All these characteristics are observed in other reanalysis data sets.

In this chapter, we have indicated that the BDC can be largely affected by the background mean wind field through the wave propagation. In the lower stratosphere, the zonal wind pro-

file is largely controlled by the diabatic heating such as short wave absorption by the ozone. The ozone distribution in the SH polar lower stratosphere has a drastic long-term change in the 20th century. In contrast, recovery of the ozone in the polar lower stratosphere is expected in the 21st century. The next chapter investigates the long-term trend of the stratospheric and mesospheric residual circulation under the ozone recovery and CO_2 increase in the 21st century using a simulation data.

第3章
本章については、5年以内に雑誌等で刊行予定のため、非公開

第４章
本章については、5年以内に雑誌等で刊行予定のため、非公開

Chapter 5

General conclusions

In this thesis several aspects of the stratospheric circulation and role of waves on the circulation were examined using a CCM, GCM, and reanalysis data sets. In particular, the gravity wave contribution to the dynamics of climatology, long-term variation, and remote connection in the circulation was focused on.

First, the wave contribution to the formation, strength, structure, and seasonal variation of the BDC is examined using a reanalysis data set (ERA-Interim). Analyses of the grobal and long-term gravity wave contribution to the residual mean circualtion is still developing field of the middle atmospheric dynamics. In particular, the estimation of the global distribution of the gravity wave forcing has been difficult because of the limitations of observations. However, the reanalysis data should include the gravity wave effects into the mean state which is approximately same as the real atmosphere by assimilations of observational data. Thus, the gravity wave contribution can be extracted from the mean state in the reanalysis data. In this study, diagnostic method of the estimation of the gravity wave forcing was used. The downward control principle indicates that the residual circulation in the TEM system is expressed by the wave forcing in the steady state. In addition, the wave forcing term is linearly decomposed of different wave component. Thus, the gravity wave contribution is indirectly estimated as a difference between the total circulation and large-scale waves. The gravity wave roles on the BDC revealed using the diagnostic analyses are summarized as

follows:

- The upwelling in the summer subtropics, which belongs to the winter deep branch of the BDC, is mainly driven by gravity waves.
- Gravity waves contribute to about 30% of the tropical upward mass flux in the lower stratosphere.
- The turnaround latitudes in the lower stratosphere cannot be formed by the large-scale waves without the gravity wave contribution in the mid-latitudes.
- Difference in the seasonal variations of the mass flux between the lower stratosphere and middle stratosphere is affected by that the contribution of gravity waves to the mass flux is dependent on the height.

These suggests importance of the gravity wave on the residual circulation even in the lower to middle stratosphere. The indirect estimation method gives grobal distribution of the gravity waves, but it is the upper limit of the gravity wave contribution. For example, the indirectly-estimated gravity wave contribution from the reanalysis data is considered to include vairous effects such as analysis and assimilation errors. In contrast, the gravity wave component detected from balloon observation, satellite instruments, etc., is spatially limited. In addition, the gravity waves cover the broad range of wavelengths in the atmosphere but the visible range of the observation is also limited depending on the instrument (the observational filter). The future study should include these effects/limitations to perform more developed analyses of the gravity waves.

Next, trend in the stratospheric circulation was investigated by focusing on the dynamical responses in the middle atmosphere to the ozone recovery and CO_2 trend in the summer SH for the 21st century using the WACCM resolving up to the lower thermosphere. The MLT response to the ozone recovery and CO_2 increase in SH summer was investigated as a confirmation of the mechanism proposed by Smith et al. (2010) which showed a MLT

response to the ozone decrease in the last half of the 20th century. Trends for temperature, zonal wind, wave forcing, and residual mean circulation are calculated for a period of 2015-2090 which includes a large CO_2 increase trend for RCP 8.5 and RCP 4.5 and no significant CO_2 trend for RCP 2.6, with similar large ozone increase trend. The ozone increase effect on the MLT trend is examined using a simulation data with RCP 4.5 scenario, and CO_2 increase effect on the MLT response is evaluated by comparisons of results from other CO_2 scenarios and by the multiple linear regression analysis.

Positive temperature trend in the polar lower stratosphere due to the ozone recovery is balanced by a trend in the easterly wind in the stratosphere. The stratospheric wind distribution modulates the gravity wave propagation into the mesosphere: more gravity waves with eastward momentum flux propagate through the stratospheric wind under the easterly trend. The increasing trend of the eastward gravity wave propagation leads to an increase of the convergence of the eastward momentum flux in the mesosphere, driving the accelerating trend of the equatorward flow. An associated acceleration of vertical flow occurs in the polar region. The strengthened upwelling below the mesopause corresponds to the cooling trend in the mesosphere. These responses to the ozone recovery are consistent with those to the ozone decrease simulated in Smith et al. (2010). The temperature trend in the polar lower thermosphere is negative (cooling), which cannot be explained only by adiabatic effects because there is no significant trend in the downwelling there. The most plausible mechanism is radiative cooling due to increase in CO_2. To investigate CO_2 effect, trends for other scenarios are calculated and compared. From the comparison, the temperature trend in the mesosphere is negative for all scenarios, but the temperature trend in the lower thermosphere is not negative for RCP2.6. This result indicates that the CO_2 effect has large contribution in the lower thermosphere and ozone effect is dominant in the mesosphere. Note that in the mesosphere the negative temperature trends are quantitatively different among three scenarios suggesting that a part of temperature trend in this region is attributed to the CO_2 variability. In addition, the mul-

tiple linear regression analysis is performed to separate the ozone and CO_2 contribution to the temperature variability. The ratio of regression coefficient also suggests that the ozone increase is important for the mesospheric variability and CO_2 trend is important for the lower thermospheric variability, which supports above discussion.

This study used three simulations of the future climate to conclude changes in the stratosphere can affect the dynamics of the MLT region. The mechanism behind the simulated responses is considered to work also in the real atmosphere. However, the ozone and CO_2 variations for the future climate will not be along with the scenarios used here. The results presented in this study should be carefully validated using the future observations. In addition, intermodel comparison is needed to investigate the model bias on the mechanism.

Finally, internal variation of the middle atmosphere was examined in terms of the dynamical pole-equator connection using high resolution (gravity wave-resolving) GCM data and a long-term reanalysis data. The reanalysis data were used in a statistical analysis to examine the SAO-PNJ interaction in austral winter.

The seasonal variation of the PNJ and SAO is investigated using the GCM data for austral winter (May, June, July, and August). The PNJ core is located at about 45°S, 60 km in May and descends with time. The easterly phase associated with SAO is located around 60 km, and also descends along the seasonal evolution. It seems that the SAO easterly and PNJ core keep same height each other in the seasonal variation. In the austral winter, planetary waves propagate into the upper stratosphere in the mid-latitudes to drive the strong poleward flow. In addition, there is gravity wave-driven strong poleward flow in the extratropical mesosphere and relatively weak poleward flow in the subtropical mesosphere. These meridional flows cause a strong upwelling in the mid-latitude upper stratosphere and lower mesosphere. This interesting features are observed in several years for the MERRA reanalysis data.

We focus on the interannual variability of the SAO and PNJ for July to examine the interaction of the SAO and PNJ variability. This analysis removes the seasonal variation so that

the SAO-PNJ interaction is easily considered. In this section, two composite analyses are performed. One is a composite on the SAO variability and another is on the PNJ variability. Since the SAO and PNJ originally has different interannual variability, both composite analyses are necessary, although the same mechanism is observed. For the former, all Julys are divided into strong SAO easterly Julys, weak SAO easterly Julys, and others. From the comparison of S-SAO and W-SAO Julys, it is found that the PNJ core tends to be located at lower altitudes when the SAO easterly is strong. This may be explained as follows: planetary waves propagating from extratropics in the troposphere is easy to break around the easterly region. Thus, in the S-SAO case the wave forcing associated with planetary waves is large and the strong poleward flow is driven. In contrast in the subtropical mesosphere, an extension of the easterly phase to the subtropics at the stratopause level affects the gravity wave propagation resulting in the equatorward flow anomaly for the S-SAOE Julys. These anomalies are responsible for the strong upwelling in the mid-latitudes. The upwelling anomaly affects the background temperature field through adiabatic cooling. Form the thermal wind balance the upper part of the PNJ is influenced. Thus, the SAO variability is possible to the PNJ location. For the latter, all Julys are divided into low PNJ Julys, high PNJ Julys, and others. This composite analysis shows that the stratospheric equatorial easterly is stronger for L-PNJ case than for H-PNJ case. In the L-PNJ Julys, more planetary waves propagate into the upper stratosphere and lower latitudes. The convergence of the planetary waves leads to the easterly acceleration which causes the strong easterly and extension of the easterly region to the higher latitudes. These two composite analyses show an evidence of the PNJ-SAO interaction. This mechanism can adjust the SAO easterly height to the PNJ core height or the PNJ core height to the SAO easterly height. The adjustment mechanism has a potential to work not only in the interannual variability but also in the seasonal variation.

In this study, we proposed a new mechanism of SAO-PNJ connection in the interannual variability from statistical analyses. In the mechanism, the strong planetary wave activity is

observed in the S-SAOE and L-PNJ Julys. The planetary wave is treated as one of the key factors of the SAO-PNJ interaction. However, the planetary waves originally come from the troposphere, and the cause of the difference in the planetary wave activity in the bottom of the stratoshere has not yet been examined. Furthermore, the planetary wave activity is generally stronger in the Northern Hemisphere. This suggests that the SAO-PNJ interaction mechanism proposed in the present study does not necessarily apply to the Northern Hemisphere. These points remain to be solved.

In this thesis, the climatology, trend, and internal variation of the stratospheric circulation were examined in terms of wave contribution. There are several remaining issues. In the analysis for trend in WACCM, the planetary wave activity trend in the mid-stratosphere was used to consider the dynamical response in the polar stratopause region. However, the tropospheric response, which modifies the planetary wave sources, was not examined. Large-scale tropospheric phenomena such as El Niño–Southern Oscillation (ENSO) are known to have impacts on the stratospheric dynamics (e.g. Taguchi and Hartmann, 2006; Randel et al., 2009). The stratospheric sudden warming (SSW) (Matsuno, 1971; Charlton and Polvani, 2007) is one of the largest events in the winter stratosphere but is neither considered in this study, which focuses on the seasonal mean state. It is well known that the stratopause can exhibit drastic change in its height when the SSW occurs (Tomikawa et al., 2012; Chandran et al., 2011; Siskind et al., 2010). McLandress and Shepherd (2009a) reported that the SSW frequency in the future climate increases due to the increase of the intrusion of the planetary waves into the stratosphere, although the SSW frequency does not increase in the future when another SSW index defined by the northern annular mode (NAM) is used. These long-term changes can affect the dynamics in the mesosphere and lower thermosphere. For the future work for comprehensive understanding of the middle atmosphere dynamics, various analyses should be made including the troposphere, stratosphere, mesosphere, and lower thermosphere, from these view points. In the analysis for the SAO-PNJ connection, the mechanism for the pole to

equator connection may be difficult to see in the Northern Hemisphere where the SSW caused by strong planetary wave activity makes the dynamics more complicated. Future analysis, including examinations of the lower stratosphere, upper stratosphere, and lower mesosphere in both the Northern and Southern Hemispheres will be required to better understand dynamics of the entire middle atmosphere and its interannual and seasonal variations. In addition, the stratospheric material circulation is originally three-dimensional and distributions of PNJ and stratopause are not uniform for zonal direction. Recently, Kinoshita and Sato (2013a,b) extended the TEM equations into a form which can express three-dimensional material circulation. Their equations are applicable to both Rossby waves and gravity waves. Three dimensional properties of the BDC should be examined in the future using such a theory.

Andrews, D. G., J. R. Holton, and C. B. Leovy, 1987: *Middle atmosphere dynamics*. Academic Press, 504 pp.

Andrews, D. G. and M. E. McIntyre, 1976: Planetary waves in horizontal and vertical shear: The generalized eliassen-palm relation and the mean zonal acceleration. *J. Atmos. Sci.*, **33**, 2031–2048, doi:10.1175/1520-0496(1976)033.

Bailey, S., A. W. Merkel, G. E. Thomas, and D. W. Rusch, 2007: Hemispheric differences in polar mesospheric cloud morphology observed by the Student Nitric Oxide Explorer. *J. Atmos. Sol. Terr. Phys.*, **69**, 1407–1418.

Baldwin, M. P., et al., 2001: The Quasi-Biennial Oscillation. *Rev. Geophys.*, **39**, 179–229, doi:10.1029/1999RG000073.

Benze, S., C. E. Randall, B. Karlsson, V. L. Harvey, M. T. DeLand, G. E. Thomas, and E. P. Shettle, 2012: On the onset of polar mesospheric cloud seasons as observed by SBUV. *J. Geophys. Res.*, **117**, D07 104, doi:10.1029/2011JD017350.

Beres, J. H., M. J. Alexander, and J. R. Holton, 2002: Effects of tropospheric wind shear on the spectrum of convectively generated gravity waves. *J. Atmos. Sci.*, **59**, 1805–1824, doi:10.1175/1520-0469.

Beres, J. H., M. J. Alexander, and J. R. Holton, 2004: A method of specifying the gravity wave spectrum above convection based on latent heating properties and background wind. *J. Atmos. Sci.*, **61**, 324–337.

Brewer, A. W., 1949: Evidence for a world circulation provided by the measurements of helium and water vapour distribution in the stratosphere. *Q. J. R. Meteor. Soc.*, **75**, 351–363.

Butchart, N., J. Austin, J. R. Knight, A. A. Scaife, and M. L. Gallani, 2000: The response of the stratospheric climate to projected changes in the concentrations of well-mixed greenhouse gases from 1992 to 2051. *J. Climate*, **13**, 2142–2159.

Butchart, N., et al., 2006: Simulations of anthropogenic change in the strength of the Brewer-

Dobson circulation. *Clim. Dyn.*, **27**, 727–741, doi:10.1007/s00382-006-0162-4.

Butchart, N., et al., 2010: Chemistry-climate model simulations of twenty-first century stratospheric climate and circulation changes. *J. Climate*, **23**, 5349–5374, doi: 10.1175/2010JCLI3404.1.

Chandran, A., R. L. Collins, R. R. Garcia, and D. R. Marsh, 2011: A case study of an elevated stratopause generated in the whole atmosphere community climate model. *Geophys. Res. Lett.*, **38**, L08 804, doi:10.1029/2010GL046566.

Charlton, A. J. and L. M. Polvani, 2007: A new look at stratospheric sudden warmings. Part I: Climatology and modeling benchmarks. *J. Climate*, **20**, 449–469.

Dee, D. P., et al., 2011: The ERA-Interim reanalysis: configuration and performance of the data assimilation system. *Q. J. R. Meteor. Soc.*, **137**, 553–597, doi:10.1002/qj.828.

Dobson, G. M. B., 1952: Ozone in the earth's atmosphere. *Endeavour*, **11**, 215–219.

Dunkerton, T. J., 1979: On the role of the Kelvin wave in the westerly phase of the semiannual zonal wind oscillation. *J. Atmos. Sci.*, **36**, 32–41.

Dunkerton, T. J., 1989: Nonlinear Hadley circulation driven by asymmetric differential heating. *J. Atmos. Sci.*, **46**, 956–974.

Dunkerton, T. J. and D. P. Delisi, 1997: Interaction of the quasi-biennial oscillation and stratopause semiannual oscillation. *J. Geophys. Res.*, **102**, 26 107–26 116.

Fritts, D. C. and G. D. Nastrom, 1992: Sources of mesoscale variability of gravity waves. Part II: frontal, convective, and jet stream excitation. *J. Atmos. Sci.*, **49**, 111–127.

Garcia, R. R. and B. A. Boville, 1994: Downward control of the mean meridional circulation and temperature distribution of the polar winter stratosphere. *J. Atmos. Sci.*, **51**, 2238–2245.

Garcia, R. R., T. J. Dunkerton, R. S. Lieberman, and R. A. Vincent, 1997: Climatology of the semiannual oscillation of the tropical middle atmosphere. *J. Geophys. Res.*, **102**, 26 019–26 032.

Garcia, R. R., D. R. Marsh, D. E. Kinnison, B. A. Boville, and F. Sassi, 2007: Simulation

of secular trends in the middle atmosphere, 1950-2003. *J. Geophys. Res.*, **112**, D09 301, doi:10.1029/2006JD007485.

Garcia, R. R. and W. J. Randel, 2008: Acceleration of the Brewer-Dobson circulation due to increases in greenhouse gases. *J. Atmos. Sci.*, **65**, 2731–2739, doi:10.1175/2010JAS3527.1.

Haynes, P. H., C. J. Marks, M. E. McIntyre, T. G. Shepherd, and K. P. Shine, 1991: On the ”downward control” of extratropical diabatic circulations by eddy-induced mean zonal forces. *J. Atmos. Sci.*, **48**, 651–678.

Hines, C. P., 1997: Doppler-spread parameterization of gravity-wave momentum deposition in the middle atmosphere. Part 2: Broad and quasi monochromatic spectra and implementation. *J. Atmos. Sol. Terr. Phys.*, **59**, 387–400.

Hirota, I., 1978: Equatorial waves in the upper atmosphere and mesosphere in relation to the semiannual oscillation of the zonal wind. *J. Atmos. Phys.*, **35**, 714–712.

Hirota, I., 1980: Observational evidence of the semiannual oscillation in the tropical middle atmosphere: A review. *Pure Appl. Geophys.*, **118**, 217–238.

Hitchman, M. H. and C. B. Leovy, 1986: Evolution of the zonal mean state in the equatorial middle atmosphere during October 1978-May 1979. *J. Atmos. Sci.*, **43**, 3159–3176.

Holton, J. R., 1990: On the global exchange of mass between the stratosphere and troposphere. *J. Atmos. Sci.*, **47**, 392–395.

Holton, J. R. and G. J. Hakim, 2013: *An introduction to dynamic meteorology*. Academic Press.

Holton, J. R. and H. C. Tan, 1980: The influence of the equatorial quasi-biennial oscillation on the global circulation at 50 mb. *J. Atmos. Sci.*, **37**, 2200.

Holton, J. R. and H. C. Tan, 1982: The quasi-biennial oscillation in the northern hemisphere lower stratosphere. *J. Meteor. Soc. Japan*, **60**, 140–148.

Hoskins, B. J., 1982: The mathematical theory of frontgenesis. *Annu. Rev. Fluid Mech.*, **14**, 131–151.

Kawatani, Y., S. Watanabe, K. Sato, T. J. Dunkerton, S. Miyahara, and M. Takahashi, 2010: The roles of equatorial trapped waves and internal inertia-gravity waves in driving the quasi-biennial oscillation. Part I: Zonal mean wave forcing. *J. Atmos. Sci.*, **67**, 963–980, doi: 10.1175/2009JAS3222.1.

Kinnison, D. E., et al., 2007: Sensitivity of chemical tracers to meteorological parameters in the mozart-3 chemical transport 25 model. *J. Geophys. Res.*, **112**, D20 302, doi: 10.1029/2006JD007879.

Kinoshita, T. and K. Sato, 2013a: A formulation of three-dimensional residual mean flow applicable both to inertia-gravity waves and to Rossby waves. *J. Atmos. Sci.*, **70**, 1577–1602, doi:10.1175/JAS-D-12-0137.1.

Kinoshita, T. and K. Sato, 2013b: A formulation of unified three-dimensional wave activity flux of inertia-gravity waves and Rossby waves. *J. Atmos. Sci.*, **70**, 1603–1615, doi: 10.1175/JAS-D-12-0138.1.

Kobayashi, S., et al., 2015: The JRA-55 Reanalysis: General specifications and basic characteristics. *J. Meteor. Soc. Japan*, **93**, doi:10.2151/jmsj.2015-001.

Li, F., J. Austin, and J. Wilson, 2008: The strength of the Brewer-Dobson circulation in a changing climate. *J. Climate*, **21**, 40–57, doi:10.1175/2007JCLI1663.1.

Lindzen, R. S., 1981: Turbulence and stress owing to gravity wave and tidal breakdown. *J. Geophys. Res.*, **86**, 9707–9714.

Lossow, S., C. McLandress, A. I. Jonsson, and T. G. Shepherd, 2012: Influence of the Antarctic ozone hole on the polar mesopause region as simulated by the Canadian Middle Atmosphere Model. *J. Atmos. Solar Terr. Phys.*, **74**, 111–123, doi:10.1016/j.jastp.2011.10.010.

Manney, G. L., et al., 2008: The evolution of the stratopause during the 2006 major warming: Satellite data and assimilated meteorological analyses. *J. Geophys. Res.*, **113**, D11, doi: 10.1029/2007JD009097.

Marsh, D. R., M. J. Mills, D. E. Kinnison, J. Lamarqu, N. Calvo, and L. M. Polvani, 2013:

Climate change from 1850 to 2005 simulated in CESM1(WACCM). *J. Climate*, **26**, 7372–7391, doi:10.1175/JCLI-D-12-00558.1.

Matsuno, T., 1971: A dynamical model of stratospheric warmings. *J. Atmos. Sci.*, **28**, 1479–11 494.

McFarlane, N. A., 1987: The effect of orographically excited gravity wave drag on the general circulation of the lower stratosphere and troposphere. *J. Atmos. Sci.*, **44**, 1775–1800.

McLandress, C. and T. G. Shepherd, 2009a: Impact of climate change on stratospheric sudden warmings as simulated by the Canadian Middle Atmosphere Model. *J. Climate*, **22**, 5449–5463, doi:10.1175/2009JCLI3069.1.

McLandress, C. and T. G. Shepherd, 2009b: Simulated anthropogenic changes in the Brewer-Dobson circulation, including its extension to high latitudes. *J. Climate*, **22**, 1516–1540, doi:10.1175/2008JCLI2979.1.

Miller, J. E., 1948: On the concept of frontgenesis. *J. Atmos. Sci.*, **5**, 169–171.

Miyazaki, K., S. Watanabe, Y. Kawatani, M. Takahashi, and K. Sato, 2010: Transport and mixing in the extratropical tropopause region in a high-vertical-resolution GCM. Part I: Potential vorticity and heat budget analysis. *J. Atmos. Sci.*, **67**, 1293–1314, doi:10.1175/2009JAS3221.1.

Moss, R. H., et al., 2010: The next generation of scenarios for climate change research and assessment. *Nature*, **463**, 747–756, doi:10.1038/nature08823.

Okamoto, K., K. Sato, and H. Akiyoshi, 2011: A study on the formation and trend of the Brewer-Dobson circulation. *J. Geophys. Res.*, **116**, D10 117, doi:10.1029/2010JD014953.

Peña-Ortiz, C., H. Schmidt, M. A. Giorgetta, and M. Keller, 2010: QBO modulation of the semiannual oscillation in MAECHAM5 and HAMMONIA. *J. Geophys. Res.*, **115**, D21, doi:10.1029/2010JD013898.

Plumb, R. A., 2002: Stratospheric transport. *J. Meteor. Soc. Japan*, **80**, 793–809.

Randel, W. J., R. R. Garcia, N. Calvo, and D. Marsh, 2009: ENSO influence on zonal mean

temperature and ozone in the tropical lower stratosphere. *Geophys. Res. lett.*, **36**, D15 822, doi:10.1029/2009GL039343.

Randel, W. J., F. Wu, J. M. Russell III, A. Roche, and J. W. Waters, 1998: Seasonal cycles and qbo variations in stratospheric CH_4 and H_2O observed in UARS HALOE data. *J. Atmos. Sci.*, **55**, 163–185.

Reed, R. J., 1962: Some features of the annual temperature regime in the tropical stratosphere. *Mon. Wea. Rev.*, **90**, 211–215.

Reed, R. J., W. J. Campbell, A. Rasmussen, and D. G. Rogers, 1961: Evidence of a downward-propagating, annual wind reversal in the equatorial stratosphere. *J. Geophys. Res.*, **66**, 813–818, doi:10.1029/JZ066i003p00813.

Richter, J. H., F. Sassi, and R. R. Garcia, 2010: Toward a physically based gravity wave source parameterization in a general circulation model. *J. Atmos. Sci.*, **67**, 136–156, doi:10.1175/2009JAS3112.1.

Rienecker, M. M., et al., 2011: MERRA: NASA's Modern-Era Retrospective Analysis for Research and Applications. *J. Climate*, **24**, 3624–3648, doi:10.1175/JCLI-D-11-00015.1.

Saha, S., et al., 2010: The NCEP climate forecast system reanalysis. *Bull. Amer. Meteor. Soc.*, **91**, 1015–1057, doi:10.1175/2010BAMS3001.1.

Salby, M. L. and R. R. Garcia, 1987: Transient response to localized episodic heating in the tropics. *J. Atmos. Sci.*, **44**, 458–498, doi:10.1175/1520-0469(1987)044¡0458:TRTLEH¿2.0.CO;2.

Sato, K. and T. J. Dunkerton, 1997: Estimates of momentum flux associated with equatorial Kelvin and gravity waves. *J. Geophys. Res.*, **102**, 26 247–26 261.

Sato, K., S. Tateno, S. Watanabe, and Y. Kawatani, 2012: Gravity wave characteristics in the southern hemisphere revealed by a high-resolution middle-atmosphere general circulation model. *J. Atmos. Sci.*, **69**, 1378–1396, doi:10.1175/JAS-D-11-0101.1.

Sato, K., S. Watanabe, Y. Kawatani, Y. Tomikawa, K. Miyazaki, and M. Takahashi, 2009: On the origins of mesospheric gravity waves. *Geophys. Res. Lett.*, **36**, L19 801, doi:

10.1029/2009GL039908.

Shepherd, T. G. and C. McLandress, 2011: A robust mechanism for strengthening of the Brewer-Dobson circulation in response to climate change: Critical-layer control of subtropical wave breaking. *J. Atmos. Sci.*, **68**, 784–797, doi:10.1175/2010JAS3608.1.

Siskind, D. E., S. D. Eckermann, J. P. McCormack, L. Coy, K. W. Hoppel, and N. L. Baker, 2010: Case studies of the mesospheric response to recent minor, major, and extended stratospheric warmings. *J. Geophys. Res.*, **115**, D00N03, doi:10.1029/2010JD014114.

Smith, A. K., R. R. Garcia, D. R. Marsh, D. E. Kinnison, and J. H. Richter, 2010: Simulations of the response of mesospheric circulation and temperature to the Antarctic ozone hole. *Geophys. Res. Lett.*, **37**, L22 803, doi:10.1029/2010GL045255.

Solomon, S., 1999: Stratospheric ozone depletion: A review of concepts and history. *Rev. Geophys.*, **37**, 275–316, doi:1999RG900008.

Taguchi, M. and D. L. Hartmann, 2006: Increased occurrence of stratospheric sudden warmings during El Niño as simulated by WACCM. *J. Climate*, **19**, 324–332, doi:10.1175/JCLI3655.1.

Thompson, D. W. and S. Solomon, 2002: Interpretation of recent southern hemisphere climate change. *Science*, **296**, 895–899, doi:10.1126/science.1069270.

Tomikawa, Y., K. Sato, S. Watanabe, Y. Kawatani, K. Miyazaki, and M. Takahashi, 2008: Wintertime temperature maximum at the subtropical stratopause in a T213L256 GCM. *J. Geophys. Res.*, **113**, D17 117, doi:10.1029/2008JD009786.

Tomikawa, Y., K. Sato, S. Watanabe, Y. Kawatani, K. Miyazaki, and M. Takahashi, 2012: Growth of planetary waves and the formation of an elevated stratopause after a major stratospheric sudden warming in a T213L256 GCM. *J. Geophys. Res.*, doi:10.1029/2011JD017243.

Uppala, S. M., et al., 2005: The ERA-40 re-analysis. *Q. J. R. Meteor. Soc.*, **131**, 2961–3012, doi:10.1256/qj.04.176.

van Vuuren, D. P., et al., 2011: The representative concentration pathways: an overview. *Climatic Change*, **109**, 5–31, doi:10.1007/s10584-011-0148-z.

Watanabe, S., Y. Tomikawa, K. Sato, Y. Kawatani, K. Miyazaki, and M. Takahashi, 2008: General aspects of a T213L256 middle atmosphere general circulation model. *J. Geophys. Res.*, **113**, D12 110, doi:10.1029/2008JD010026.

Watanabe, S., Y. Tomikawa, K. Sato, Y. Kawatani, K. Miyazaki, and M. Takahashi, 2009: Simulation of the eastward 4-day wave in the Antarctic winter mesosphere using a gravity wave resolving general circulation model. *J. Geophys. Res.*, **114**, D16 111, doi:10.1029/2008JD011636.

Xu, J., H.-L. Liu, W. Yuan, A. K. Smith, R. G. Roble, C. J. Mertens, J. M. Russell III, and M. G. Mlynczak, 2007: Mesopause structure from Thermosphere, Ionosphere, Mesosphere, Energetics, and Dynamics (TIMED)/Soundings of the Atmosphere Using Broadband Emission Radiometry (SABER) observations. *J. Geophys. Res.*, **112**, D09 102, doi:10.1029/2006JD007711.

Zhang, F., 2004: Generation of mesoscale gravity waves in upper-tropospheric jet-front systems. *J. Atmos. Sci.*, **61**, 440–457, doi:10.1175/1520-0469(2004)061¡0440:GOMGWI¿2.0.CO;2.

Acknowledgments

The author is most grateful to the supervisor Prof. Kaoru Sato for her patient and strict guidance and helpful suggestions in performing the present study.

He deeply acknowledges the members of this dissertation committee, Profs. Masaaki Takahashi, Masahide Kimoto, Masaki Satoh, and Tomoki Tozuka. Thanks are also due to Prof. Masatomo Fujiwara and Drs. Shingo Watanabe, Yoshio Kawatani, Yoshihiro Tomikawa, and for many important advises and suggestions.

Special thanks are given to Drs. Rolando Garcia, Anne Smith, and Danniel Marsh for fruitful discussions and suggestions while the author's stay in NCAR.

He appreciates suggestive discussions by Profs. Makoto Koike, Hiroaki Miura, Norihiko Sugimoto, and Toshiyuki Hibiya. He would like to express his gratitude to members of the atmosphere dynamics laboratory for their discussions: Dr. Takenari Kinoshita, Mr. Chikara Tsuchiya, Mr. Masashi Kohma, Mr. Masahiro Nomoto, Mr. Yuuki Yasuda, Mr. Ryosuke Shibuya, Mr. Akihiro Masuda, Mr. Arata Amemiya, and Mr. Soichiro Hirano.

Part of this study was supported by the Overseas Internship Program for Outstanding Young Earth and Planetary Researchers (OIYR Program) as a part of the Japan Society for the Promotion of Science (JSPS) Institutional Program for Young Researcher Overseas Visits, and also supported by Grant-in-Aid for Research Fellow (24-487 10405) of the JSPS. The CESM project is supported by the National Science Foundation and the Office of Science (BER) of the U.S. Department of Energy. The GFD-DENNOU library was used for graphical output.